5-2021

Joint spacing in the Caples Lake granodiorite of the Sierra Nevada Batholith in Eldorado National Forest, California: A comparative analysis of joint sets and data resolution

Jimmy Wood
wood1466@umn.edu

UNIVERSITY OF NEBRASKA - OMAHA

COLLEGE OF ARTS AND SCIENCES

DEPARTMENT OF GEOGRAPHY/GEOLOGY

Joint spacing in the Caples Lake granodiorite of the Sierra Nevada Batholith in Eldorado National Forest, California: A comparative analysis of joint sets and data resolution

A Senior Thesis

by

Jimmy Wood

Submitted in partial fulfillment

of the requirements

for the degree of

Bachelor of Science

Spring 2021

ABSTRACT

Joints are the most common deformation structure in the Earth's upper crust and exert a significant influence on structural stability, landscape morphology, and fluid flow . Therefore, a greater understanding of fracture parameters (e.g., length, aperture, etc.) allows us to more accurately predict their presence, persistence, and prevalence, in the subsurface . We study the fracture spacing of two sub-orthogonal joint sets—66 NE-246 SW and 330 NW-150 SE—in the Caples Lake granodiorite of the Sierra Nevada Batholith, California. Specifically, we investigate 1) their spacing distributions with a keen interest in power-law (fractal) spacing, 2) distribution comparisons between master and cross joints, and 3) the usability of Google Earth datasets in joint spacing analyses. Spacing was calculated from position data obtained in the field and on Google Earth along one-dimensional traverses orthogonal to the mean joint strike of a set , with a target sample size of 100 for a stable fractal dimension. We tested fractal behavior through log-log cumulative frequency vs. spacing plots , determined the spacing distribution with the Chi-squared (χ^2) goodness-of-fit test, and compared distributions with the Kolmogorov-Smirnov statistic and the Coefficient of Variation . All four datasets exhibit non-fractal behavior and can instead be better described by lognormal or gamma distributions. This may be the result of sampling biases such as truncation or censoring , which can be possibly overcome with greater sample sizes and extending our lower limit of measurement an order of magnitude into the millimeters. Master and cross joints have slightly different distributions as expected from joints of different age; however, this relationship is still unclear and should be further explored with a greater sample size and less opportunistic sampling scheme that encourages shorter traverses further upslope on an outcrop. Google Earth datasets were significantly inadequate for joint spacing analyses. As expected, they routinely underestimate smaller spacings and as a result generate larger, artificial spacings, and distributions of shifted form and position. Within fracture analysis, Google Earth should remain a tool for field site reconnaissance and mapping only.

ACKNOWLEDGEMENTS

As with any academic achievement I have many thanks to give. Dr. Maher, thank you for kicking off this work by inviting me to conduct field work last summer. I was disappointed for having to miss out an in-person field camp but have surely ended up in something much better and have greatly appreciated all the work you have put into helping me through the research process throughout this past academic year. You have taught me much about working in the field, its sometimes-unrelenting discomfort and its wholly redeeming qualities. Related, I must also thank Sarah Morse for welcoming me on that trip, so central to fulfilling your visions of a senior thesis, and unknowingly, my own. Thank you Dr. Dere for helping me keep momentum throughout this last semester, for the invaluable feedback, and for the constant reminders that some progress, no matter how little, is still work in the right direction. I have reminded myself of that every day. Finally, I find it only right that I attempt to thank the Geology department as a whole. I have loved each and every one of your class's that I have had or chosen to take. I have been left with an even greater enthusiasm for, and motivation to learn, all things Earth Science because of what I learned in those classrooms. This paper is the culmination of all your teachings, and all my hard work, so I hope it's pretty good. This work was funded by the American Chemical Society Petroleum Research Fund.

TABLE OF CONTENTS

INTRODUCTION

In virtually all rock types and all tectonic environments we find steeply dipping fractures (Pollard & Aydin, 1988). In general, rock fractures comprise one of the five primary categories of deformation structures that permeate the Earth's lithosphere (Pollard & Martel, 2020). Their often (and rightly) proclaimed ubiquity and variability present a near inexhaustible research focus for the structural geologist, or student, with even a slight interest in fracture analysis (Segall & Pollard, 1983). These features can be simply defined as any discontinuity within a geologic material that has developed in response to stress (Bonnet et al., 2001). Generally, all fractures share these three fundamental characteristics (Pollard & Aydin, 1988).

1. They are largely distinguished by two parallel surfaces called the fracture faces or walls.
2. These faces are approximately planar or sub-planar to each other.
3. The faces' displacement—separation perpendicular to the fracture face—is very narrow compared to the overall length of the fracture (Fossen, 2016; Pollard & Aydin, 1988) .

While fractures observed in nature largely adhere to these characteristics, their exact expression can be highly variable, both between adjacent fractures and along the length of an individual fracture. For example, one fracture face may only be locally approximated by a planar surface, while at a larger scale is better characterized as curvi-planar.

Fractures are the result of brittle deformation—a trademark of the upper crust environment—and form where stresses exceed the local rupture strength of a rock (Fossen, 2016). These stresses may be of local to regional extent and are characterized as either external or internal. Examples of external stresses include tectonism, overburden accumulation or removal, those related to topography, and changes in fluid pressures, while the latter may include thermal and residual stresses, as well as those related to diagenetic processes. The threshold to cause rupture depends on the rock's mineralogy and composition, its confining pressure—related to the depth of burial—and, perhaps most importantly, randomly distributed and oriented microdefects in the rock itself (Fossen, 2016). This last point may explain why fractures form where they do. Griffith (1924) suggested that natural rocks and the crystals that form them are naturally imperfect (Fossen, 2016; Pollard & Aydin, 1988). Thus, rocks likely contain an abundance of flaws and cracks on the micro-scale. Other features such as pore space, voids, and grain boundaries, can all be considered microcracks in this context. Their presence weakens rock and if oriented near the minimum stress direction, assist in fracturing as shown in **Figure 1** (Fossen, 2016).

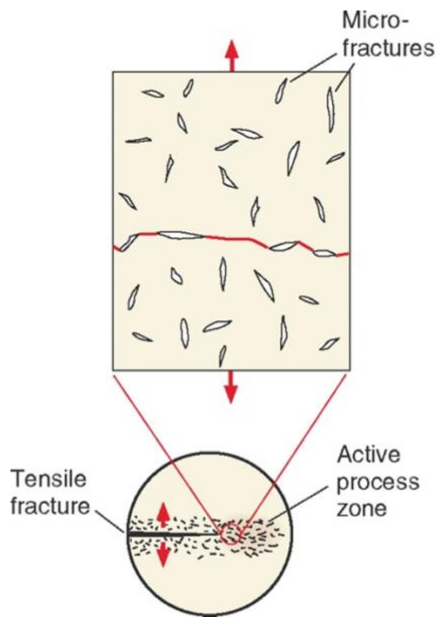

Figure 1. Growth of a tensile fracture through the linking of microfractures. Adapted from Fossen, (2016).

The current classification scheme separates fractures into three primary modes, distinguished by the relative displacement of paired fracture faces (**Figure 2**) (Fossen, 2016).

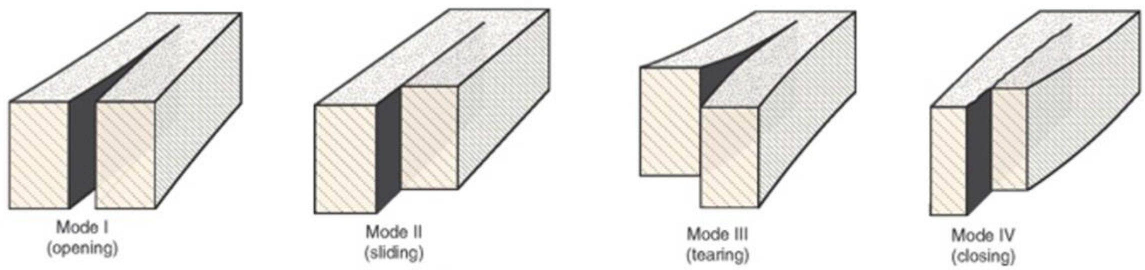

Figure 2. Primary fracture Modes I-III, along with Mode IV. Adapted from Fossen, (2016).

Mode I, or opening mode, involves a displacement normal to the walls of the fracture. Mode II and III both describe wall parallel displacements—modeling faults—but with different relative motion (Bonnet et al., 2001; Fossen, 2016). A fourth, closing mode, encompasses contraction features such as styolites, but is not a primary focus of this work. These are merely end members of a fracture continuum as modes can also combine to create hybrid cracks (Fossen, 2016).

The focus of this work is opening mode or extension fractures (Fossen, 2016). The most common type has small to moderate displacements and are called joints—for the purpose of this work we will use fracture and joint interchangeably (Pollard & Aydin, 1988). As previously mentioned, almost all rocky outcrops exhibit joints (Fossen, 2016). They occur as a series of sub-parallel fractures that define a joint set, under the assumption that they have formed under the influence of the same stress conditions during the same fracture episode (Pollard & Aydin, 1988). All joints within a given set largely share the same morphology and orientation. Natural joint patterns are commonly comprised of more than one set—usually up to three or four, with various orientations relative to each other—which together define a joint system (Fossen, 2016). These may form many varying patterns, of which some examples are shown in in **Figure 3.** The physical interaction of these sets is valuable and may reveal important age relationships and distinguish fracture forming episodes. If members of one set consistently terminate against members of another, we may reasonably assume the former to be younger than the latter (Pollard & Martel, 2020).

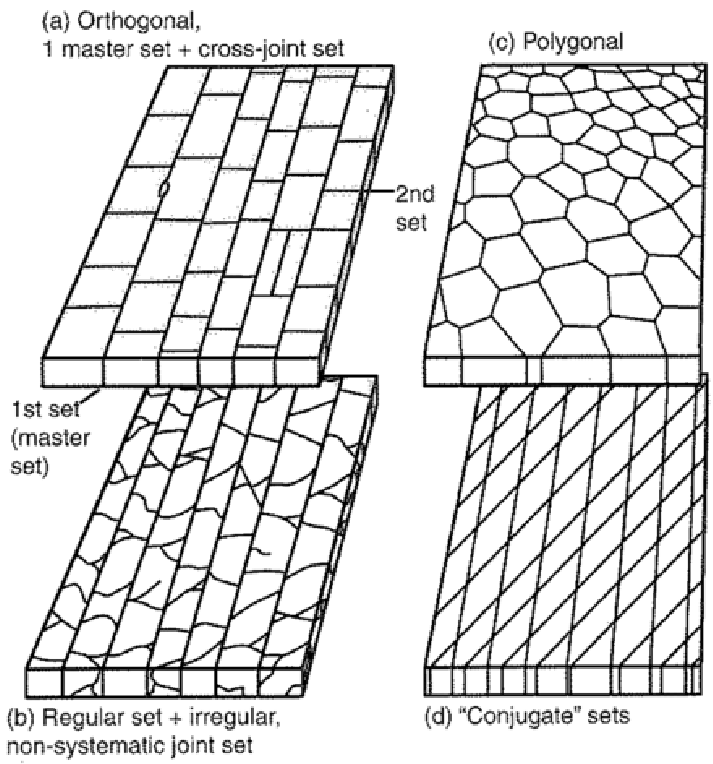

Figure 3. Examples of common joint patterns. Our field sets take the form of **a**. From Fossen, 2016.

Under the previous assumption, we infer that joint sets, having different orientations, formed under contrasting stress fields which evolve over geologic time (this may not always be the case, though, and should be corroborated with field observations) (Pollard & Martel, 2020). This record of rock deformation is of inherent interest to structural geologists (Segall & Pollard, 1983) and allows them to reconstruct paleostress conditions and unravel the history of an area (Ehlen, 2000). Jointing is also of special interest to the geomorphologist as they can greatly influence the physiography of landforms in rock cut landscapes (Ericson et al., 2004) such as coastlines, stream networks, mountain peaks, and desert mesas (Pollard & Martel, 2020).

Fracture analysis is also of practical interest to many industries central to infrastructure and natural resources. By providing secondary permeability to generally impermeable materials such as crystalline basement rocks, compacted and cemented sedimentary beds, and shales, jointing can have a significant effect on subsurface fluid flow (Fossen, 2016) (Le Garzic et al., 2011). This has implications for not only water resource management but the mining and energy industries as ore forming fluids, oil, gas, and even geothermal energy, may all be transmitted through fractures (Pollard & Aydin, 1988). As the meso- and macroscopic expression of microcracks and other defects (Fossen, 2016), joints also play a crucial role in rock deformability by physically weakening the host rock (Fossen, 2016; Pollard & Aydin, 1988); therefore, joints must be carefully investigated when planning certain engineering and development projects. If building a highway or powerplant; installing a dam, bridge, or tunnel; or attempting to ascertain the least-risk setting for a nuclear waste repository (Pollard & Aydin, 1988); knowledge of the local fracture pattern is of paramount importance. To understand the influence of fracture systems in these settings their geometrical attributes such as length, aperture, density, etc., the spatial distribution of those values, and the spatial distribution of the joints themselves must be determined (Le Garzic et al., 2011; Segall & Pollard, 1983).

Historical Perspective

The first major work on jointing (in the Geological Society of America *Bulletin*) was carried out by Becker in 1893. Observations that outcrops in the Sierra Nevada are always fractured led to the argument that orogenies could never be meaningfully discussed until the mechanical significance of jointing and faulting was understood, thus highlighting their intrinsic value; however, up until then joints were not simply ignored. Eleven years earlier, field notes left by Gilbert, conducting field work in the Great Salt Lake Desert of Utah on rectangular drainage systems in post-glacial sediments, sparked a lively debate on their origin. His claim that no "satisfactory explanation has ever been given of the origin of the jointed structure in rocks," lead to a number of contrasting suggestions from desiccation to magnetic forces. Unknown to them, this question had already been answered in Great Britain by Hopkins in 1835—almost half a century before. He interpreted joints as discontinuities caused by tensile stress (Pollard & Aydin, 1988), the general definition accepted today (Fossen, 2016). Later work by Becker (1893) and Van Hise (1896) would also yield the same conclusion (Pollard & Aydin, 1988).

Joint Spacing

The International Society of Rock Mechanics suggests eleven parameters to provide a quantitative description of fractures—spacing and orientation are the most commonly reported (Fatt, 1994). Joint spacing refers to the distance between two adjacent, sub-parallel fractures (**Figure 4**) (Ryan, 2000).

Figure 4. Joint spacing in the field (original photo, left, and interpreted, right). Black lines indicate joint traces—dotted where not certain, such as through regolith and vegetation, or for eroded faces. Red and blue lines indicate the spacing of the traced joint sets. Note how they vary, both between different fractures of the same set, and between the same two fractures along their lengths.

A large body of work has already been devoted to joint spacing in sedimentary rocks and has revealed a roughly linear relationship between spacing and layer thickness (Bai & Pollard, 1999; Ehlen, 2000), an idea which goes back to at least the late 1960s when Hobbs proposed one of the earliest theoretical models for describing joint spacing (Bai & Pollard, 1999). The linearity between bed thickness and joint spacing extends to effective layers as well—certain geometrical configurations which mechanically approximate the same response of true layers to jointing (Palmström, 1995). In this way a previously existing joint set may act as a mechanical layering who's spacing (i.e., thickness) constrains the spacing of subsequent joints (Ruf et al., 1997).

Of interest to us is the spacing distribution of an individual joint set. Various distribution patterns have been reported in the literature (National Research Council [NRC], 1996) including lognormal, gamma, and exponential , but over the past few decades it has become increasingly apparent that many fracture properties follow a power-law distribution and therefore exhibit fractal or multi-fractal behavior (Ehlen, 2000). Fractals are generally characterized by the self-similarity of some characteristic at different observation scales (Velde et al., 1991). These kind of scaling laws are promising (Bonnet et al., 2001) as they offer the extrapolation from small samples to much larger ones—e.g., outcrop scale to regional scale (Le Garzic et al., 2011)—and could greatly simplify somewhat slow sampling methods and procedures (Velde et al., 1991). Added interest in fractal behavior stems from the practical uses of fracture analysis mentioned above. The underlying controls on fracture scaling and the spacing distribution are also likely related to both the nature of the host rocks and the conditions of deformation, and so may shed light on the intricacies of fracture forming history (Gillespie et al., 2000).

Though joints are found in igneous and metamorphic rocks (Fossen, 2016) they remain much less studied than the sedimentary variety (Wong et al., 2018). This may be due to the perceived convenience of working in the more well constrained geometries, age relationships, and burial histories, of soft rocks (Fossen, 2016). Spacing in intrusive igneous rocks has been reported as nonuniform (Pollard & Aydin, 1988), but a similarly consistent relationship between spacing and rock geometry—such as spacing to layer thickness—or other traits has not yet been established. Even so, intrusive igneous rocks are ideal research targets for their relatively simple mineralogy, their, to a first approximation (Pennacchioni & Zucchi, 2013), homogenous and isotropic structure, and because they can be assumed to have responded to deformation forces in the most direct manner (Velde et al., 1991).

A primary component of this work also takes place in Google Earth. Despite an extensive array of high-resolution imagery across the globe, Google Earth has largely been relegated in the research community to mainly educational and visualization purposes; Few have actually utilized that imagery to yield quantitative data from which they plan to draw conclusions. This notion is not unprecedented. One of the first datasets believed to be produced from Google Earth imagery from Constantine and Dunne (2008) successfully predicted the size distribution of oxbow lakes along the Sacramento river (Fisher et al., 2012). Furthermore, not only does Google Earth deliver high-resolution imagery, but imagery that can be accessed on almost any computer, by almost anyone, and at the best price—free. It also opens up parts of the Earth that might preclude field work due to sheer remoteness, political conflicts, and, of course, the high cost of obtaining aerial imagery (Fisher et al., 2012) and travel. Therefore, its use as a primary dataset must be further investigated.

To further these endeavors, this work investigates joint patterns in the Sierra Nevada mountains of California, U.S.A. Here, granite plays a major role in geologic structure (Ericson et al., 2004) and we gather datasets from both the field and Google Earth. With these datasets we seek to answer three questions:

1. What are the spacing distributions of the two, dominant joint sets in our study area?
2. How do the spacing distributions of these two joint sets of apparent different age compare?
3. Do datasets collected at Google Earth scales yield the same distribution as datasets collected in the field at the outcrop scale.

BACKGROUND GEOLOGY

From the sweltering Mojave Desert to the rumbling Cascade Range (Bateman, 1968) the Sierra Nevada Mountains extend over 600 km (965 mi) along the eastern border of California following a NNE-SSW trend (Ericson et al., 2004). Together, these peaks comprise the tallest, longest, and youngest, mountain chain in the contiguous U.S (Busby et al., 2008). At the largest scale the Sierras can be approximated by an asymmetric, rigid, tilted block, sloping relatively gently to the west and much more steeply to the east, effectively isolating the Central Valley of California from the Basin and Range province, respectively (Ericson et al., 2004) (**Figure 5**).

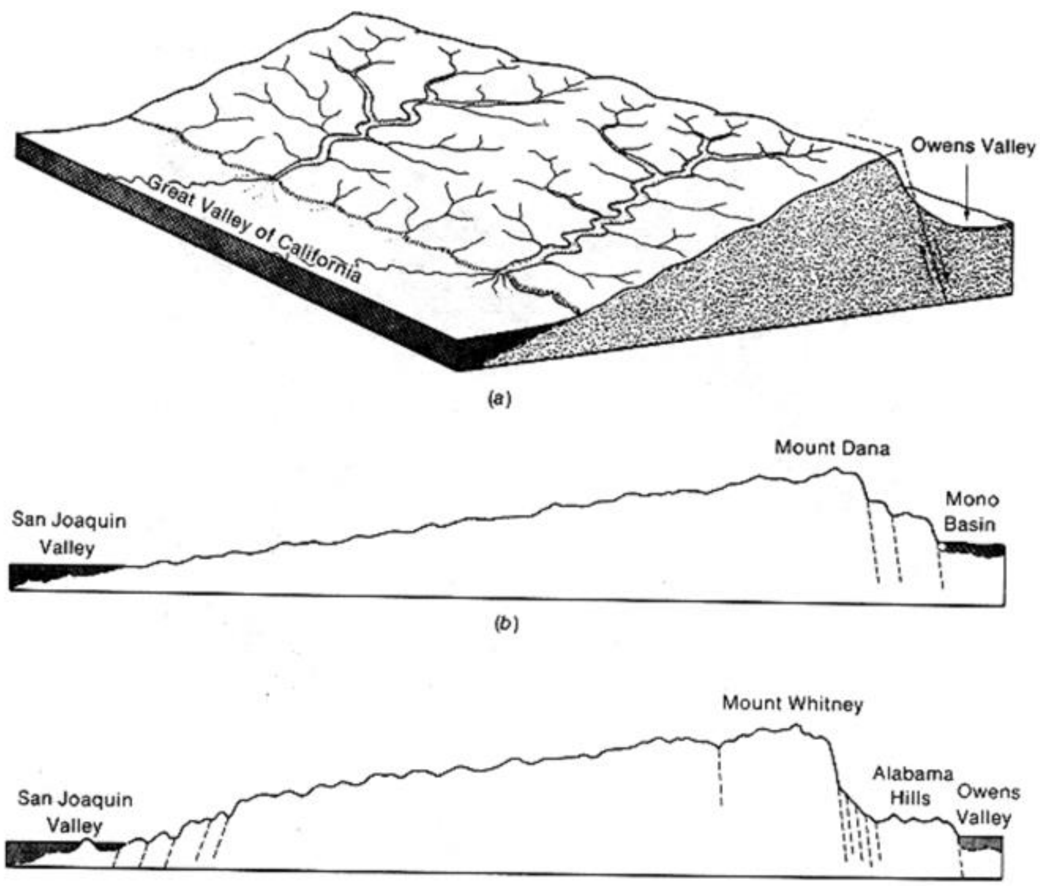

Figure 5. Large scale diagram of the Sierra Nevada Mountains highlighting fault block tilt. From "Sierra Nevada," 2012.

At the core of these mountains is the Sierra Nevada Batholith (SNB) (**Figure 6**). It is one of the largest in North America (Cecil et al., 2012) yet is more accurately described as a composite structure formed from hundreds of individual plutons (Ericson et al., 2004). These bodies—traced to the long-lived (70-120 Ma (Bateman, 1968)), island-arc (Ericson et al., 2004) subduction of the Pacific plate beneath the North American (Cecil et al., 2012)—intruded strongly deformed but weakly metamorphosed Paleozoic and Mesozoic sedimentary rocks and volcanics (Bateman, 1968). The resulting average plutonic composition largely ranges between a quartz monzonite and granodiorite, in comparable abundance (Bateman, 1968).

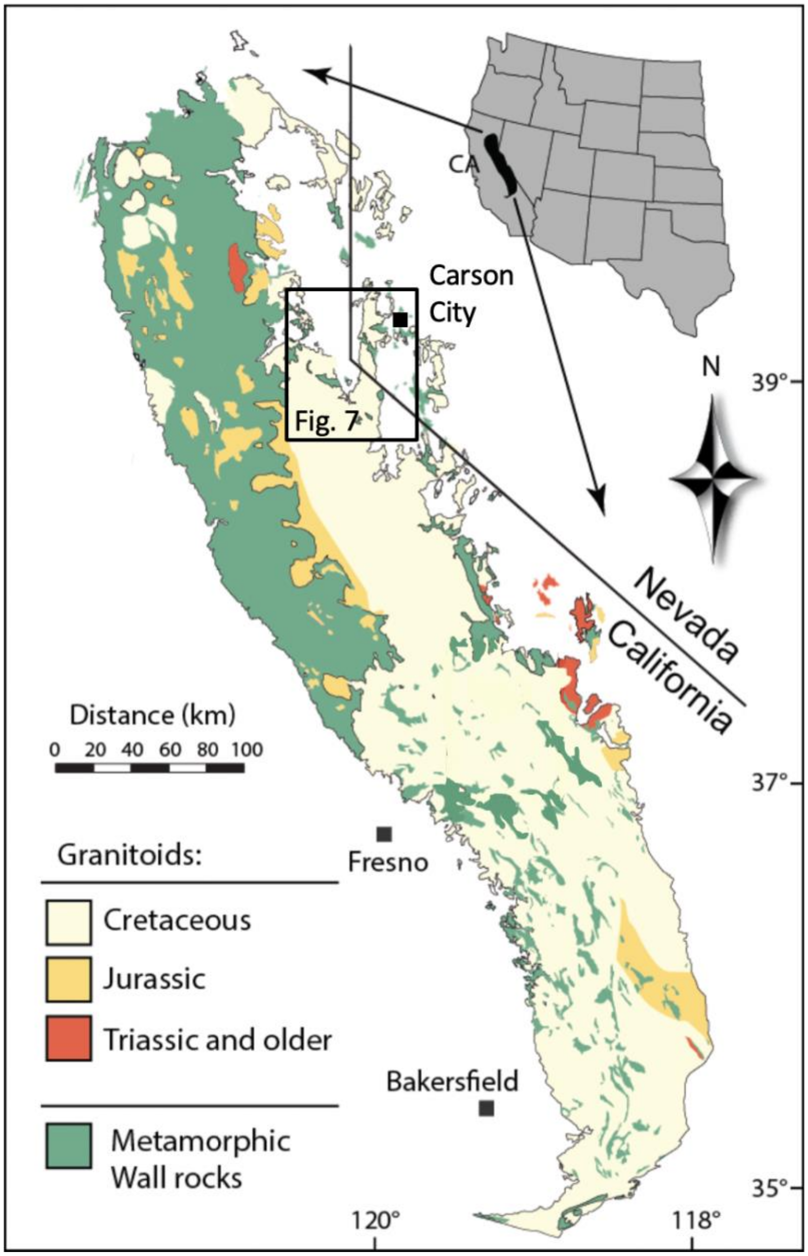

Figure 6. Generalized geologic map of the SNB. Rectangle marks boundaries of **Figure 7A**. Adapted from Sendek, (2016).

Along with rock type, other geologic and geographic factors appropriately match the SNB to our goals. During the Pleistocene Sierra Nevada peaks were extensively glaciated several times (Bateman, 1968; Ericson et al., 2004). This has left a legacy in the form of excellent outcrop exposures which not only assist with remote mapping and study site selection, but also the ease of travel, access, and the speed of data collection (Ericson et al., 2004). Excellent exposures such as these do come with drawbacks though. In sculping these outcrops glaciation and deglaciation have also led to the formation of new joints in the form of sheeting and have made all fractures more susceptible to exploitation, and subsequent alteration, via weathering and erosion. In other words, jointing in the SNB is plentiful but complicated. Steeply dipping joints (Pennacchioni & Zucchi, 2013) are also ubiquitous in the granitic part of the Sierras (Ericson et al., 2004), typically of regional extent (Segall & Pollard, 1983) with noticeably similar patterns from area to area (Ehlen, 1999). These allow for observation on a wide range of scales, from micro cracks on a thin section to lineaments extending for 10s of kilometers (Ericson et al., 2004). Thus, sample sizes can be appropriately large and an investigation of the area with aerial imagery is possible.

METHODOLOGY

Study Area & Site Description

Our field area consists of four sites in Eldorado National Forest, CA, southwest of Silver Lake, in the northern SNB. This was identified during a preliminary reconnaissance in Google Earth by Morse et al. (2020) (**Figure 7**).

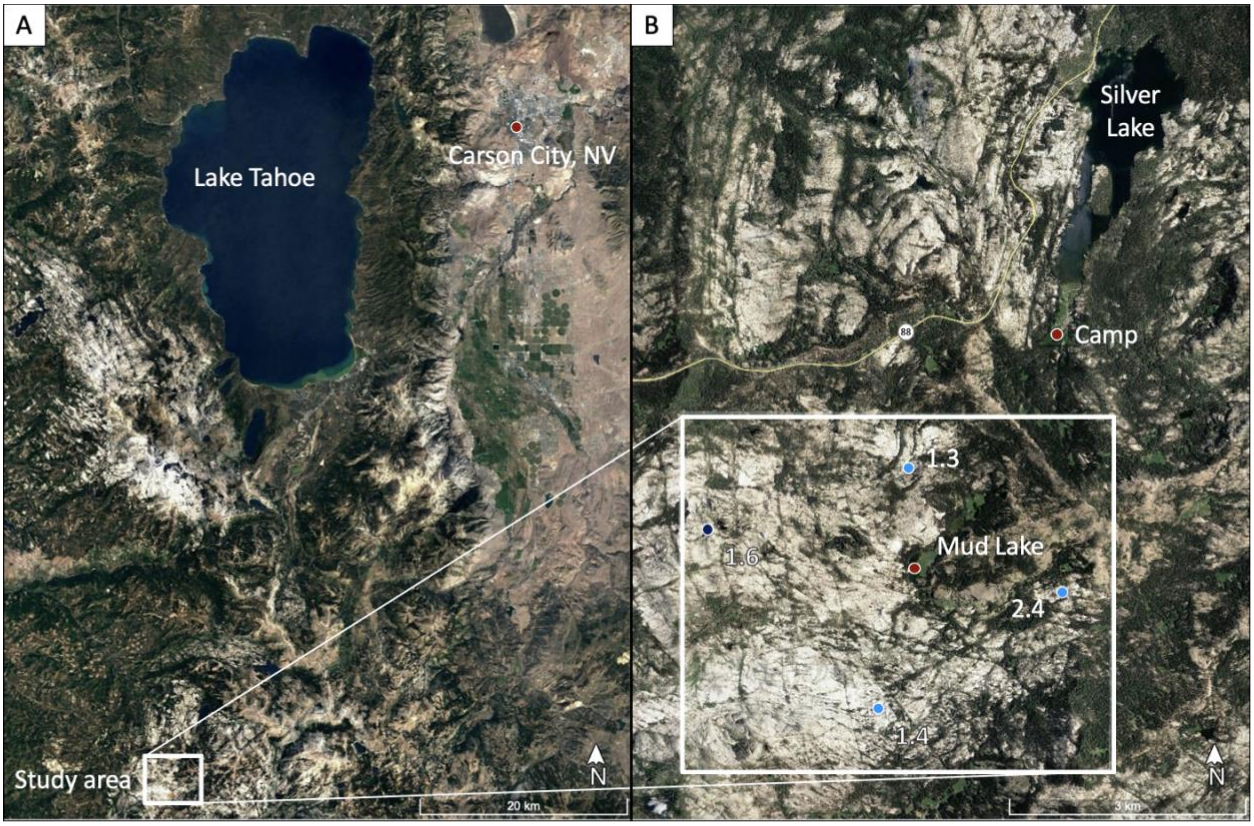

Figure 7. Study area. **A.** General location relative to Lake Tahoe and Carson City, NV**. B.** Location of four field sites—1.3, 1.4, 1.6, 2.4—and camp relative to Silver Lake and Highway 88. Light blue markers indicate sites which yielded data used in analysis. From Google Earth.

Outcrops are composed of Cretaceous plutons, of which, there are at least three major separately emplaced bodies, accompanied by several smaller ones in the surrounding area (general overview shown in **Figure 8**) (McKee et al., 1982). Our sites were solely underlain by the Caples Lake Granodiorite—the second major pluton—described as "a predominantly medium-coarse grained porphyritic hornblende biotite granodiorite," by McKee et al. (1982) during a USGS mineral resource exploration of the area. K-Ar dating carried out by Evernden and Kistler (1970) on biotite yielded 91.7 Ma and 94.3 Ma, and on hornblende, 99.6 Ma (McKee et al., 1982).

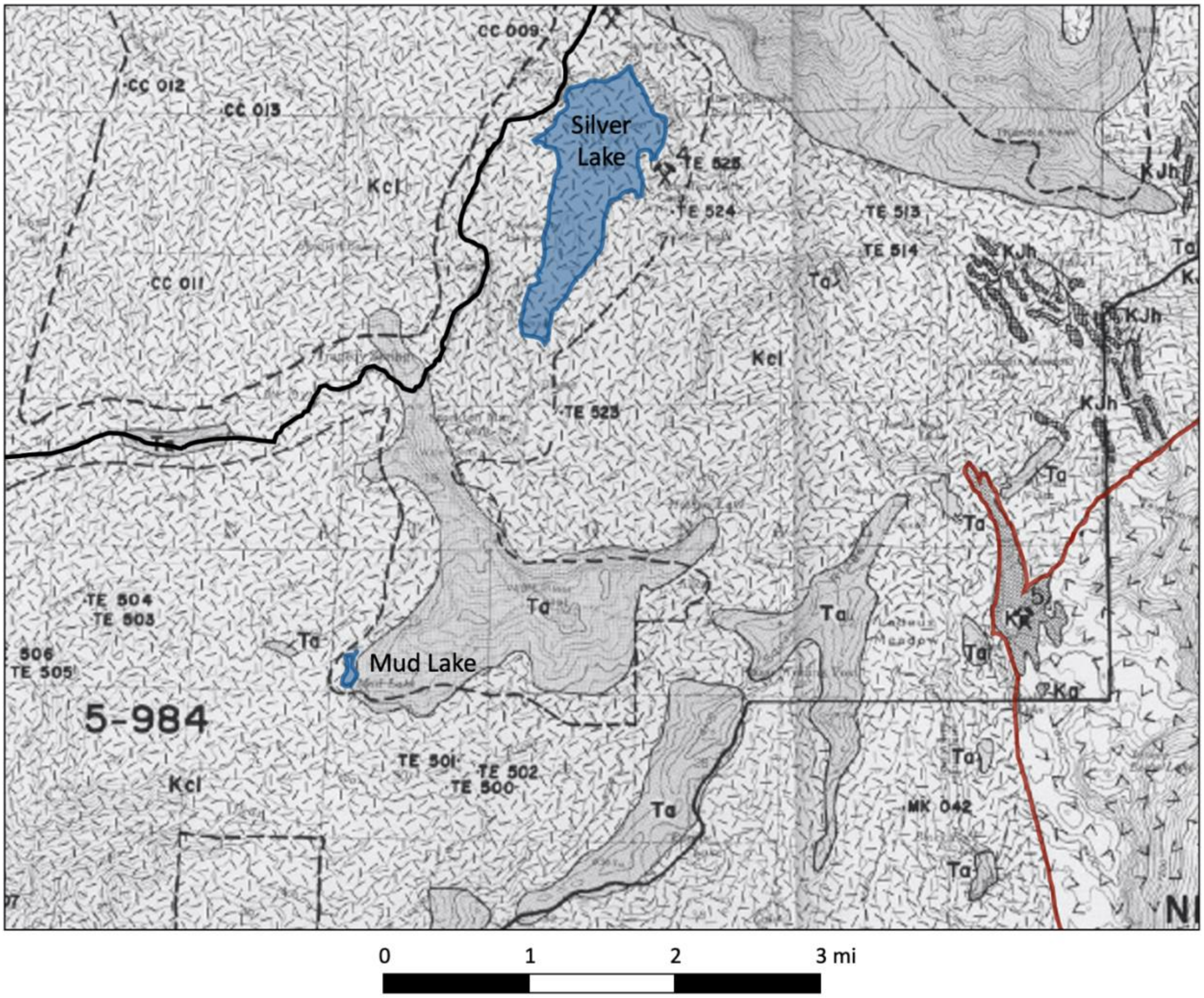

Figure 8. Geologic map of the study area. Covering the majority of this snapshot is the Caples Lake Granodiorite (Kcl) and reworked volcanics (Ta). Other regional plutons crop out to the east, outside of our study area, outlined in maroon. Adapted from McKee et al., (1982).

Within a given outcrop joints were commonly associated with a consistent suite of other sub-parallel structures, also observed elsewhere in the batholith: mineralized joints—commonly filled with epidote and chlorite (Martel et al., 1988) with narrow, bleached alteration zones (Segall & Pollard, 1983); thin, ductile shear zones (Pennacchioni & Zucchi, 2013); aplite dikes and pegmatites; and a weak magmatic foliation.

Data Collection

Field

To characterize joint spacing, joint position data was collected along a one-dimensional traverse or scanline—in this case a long measuring tape. Along the traverse, each position of intersection with a fracture (p) was recorded from which spacing (s) could be calculated through the simple relation, $s = p_j - p_i$, where the indices j and i correspond to the jth and ith fractures, respectively (Fossen, 2016). The determination of joint spacing between adjacent fractures in a set will allow us to directly determine the overall spacing distribution of our two dominant sets.

As previously mentioned, most joint sets are a part of a greater joint system; therefore, any traverse along a natural outcrop will likely intersect with fractures outside of the set of interest. To ensure a spacing distribution is representative of that set alone—the general goal—a careful sampling procedure must be followed. Here, we simply set the traverse perpendicular to the mean joint strike of one set (Fossen, 2016) and ignore all joints that are not mutually sub-perpendicular to that line (in the field this cutoff was likely around 5°-10°, to account for individual variations in joint strike). Also, the most representative dataset of this type is captured with the longest sample line. This helps eliminate sampling bias as we are likely driven to place a traverse where we perceive there to be a greater number of datapoints (e.g., a heavily fractured cluster), and thus forgoing larger swathes of unbroken rock—carrying equally insightful information. To achieve this in the field we adopt an opportunistic sampling scheme (Palinkas et al., 2013). Still, this is often unattainable due to constraints placed upon us by our equipment and the outcrop itself. Our measuring tape allowed for a maximum traverse length of 30 m. This can be extended almost indefinitely by placing the start of one sample line at the end of the previous and along the same heading, but block geometry and the presence of regolith and vegetative cover often precluded its full utilization (McCaffrey et al., 1993). Outcrops were instead sampled via a sequence of offset traverse segments—3.85 – 30 m long—forming a larger, discontinuous traverse. To eliminate confusion, we will refer to these individual sample lines as "segments" and their combined whole as the "traverse" throughout the rest of this paper. Datasets from each traverse yielded through this segmentation are considered accurate as the segments had little to no sampling overlap (McCaffrey et al., 1993). **Figure 9** shows the traverses from which data was analyzed.

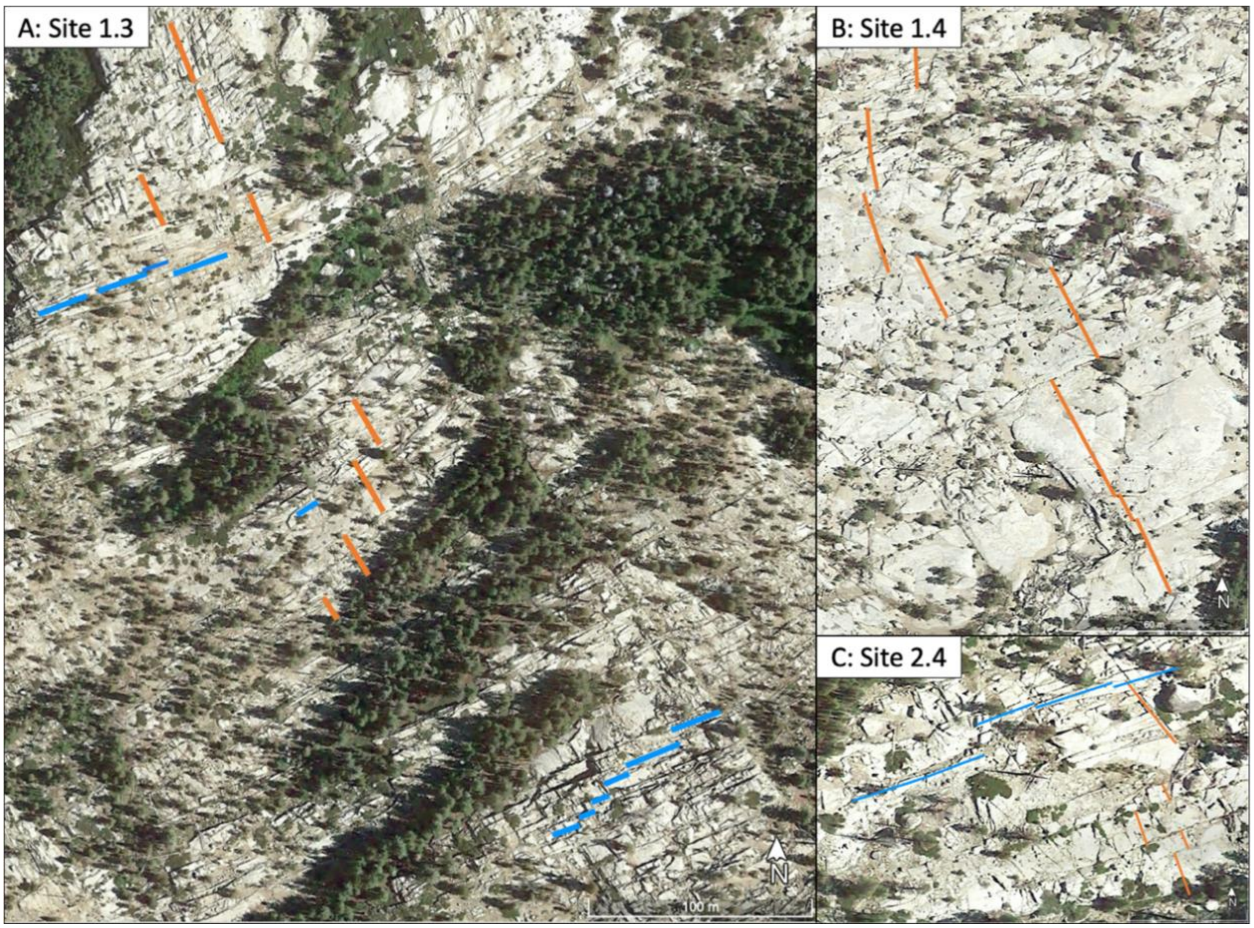

Figure 9. All analyzed traverses. Joint sets recorded distinguished by color. Scales read, **A.** 100 m, **B.** 60 m, and **C.** 30 m. From Google Earth.

Traverses were sampled until a target sample size of at least 100 spacings was achieved (Ehlen, 1999). This target represents the minimum number of measurements needed to obtain a stable fractal dimension (D)—one that does not change with an increased sample size. Until this threshold is met, the fractal dimension will vary markedly and our ability to accurately characterize a system significantly decreases (Ehlen, 2000). A similar sampling scheme was repeated for both dominant joint sets to capture the two patterns at all sites. At most, we were able to reach 93 measurements, which is considered close enough to the target value. For the 66°NE - 246° SW set (strike determined as the average of measurements along traverses), average joint spacing was sometimes large enough that only around half this number could be reached with even a 150 m traverse. Our sampling goal for that set—modified in the field, hence opportunistic—became at least 50 measurements. To overcome these limitations and more accurately capture spacing, datasets from each traverse were compiled according to joint strike into two composite datasets—one for each joint set (Gillespie et al., 2000). Lastly, joint data is only meaningful when considered with respect to joint orientation, especially when comparisons between sets are to be made (Ryan, 2000); therefore, fracture strikes were measured with a Brunton compass along with dip (Ehlen, 1999).

Google Earth imagery

To directly compare methods of data collection we laid out all segments of each traverse from the field in Google Earth. Generated traverses were calibrated with GPS coordinates and heading data taken from each segment to ensure accuracy. Sampling procedures from the field were repeated and adapted to the imagery. At the outcrop and sub-outcrop scales all linear features crossing the traverse at the appropriate angles were assumed to be structural discontinuities as done by Ericson et al. (2004). Still, due to resolution it is likely that some of these assumed individual discontinuities instead represent narrow zones of dense jointing (Ericson et al., 2004). No later corrections were made to account for this discrepancy as a direct comparison of the methods is our primary concern. Resolution is further exacerbated by the above-mentioned outcrop constraints, namely erosive and vegetative cover. All relevant datasets collected in the field and Google Earth will be included in **Appendix A**. Our procedure, including data extraction from Google Earth and conversion to a workable format, will also be included in **Appendix B**.

Data Analysis

Joint spacing was first calculated via the above equation for all segments ($s = p_j - p_i$). The following analyses—explained for field data first—were carried out for traverse data and then for composite datasets to capture any variation and discrepancies between the samples and the population. A more detailed description of the statistical analyses will follow in **Appendix C**.

Fractal analysis

Fractal behavior was investigated first as it follows a simple procedure. On a log-log plot of cumulative frequency vs. joint parameter—in this case spacing—fractal behavior will yield a straight line with a slope of $-D$ (fractal dimension) (**Figure 10**) (Bonnet et al., 2001; Ehlen, 2000; Le Garzic et al., 2011; McCaffrey et al., 1993).

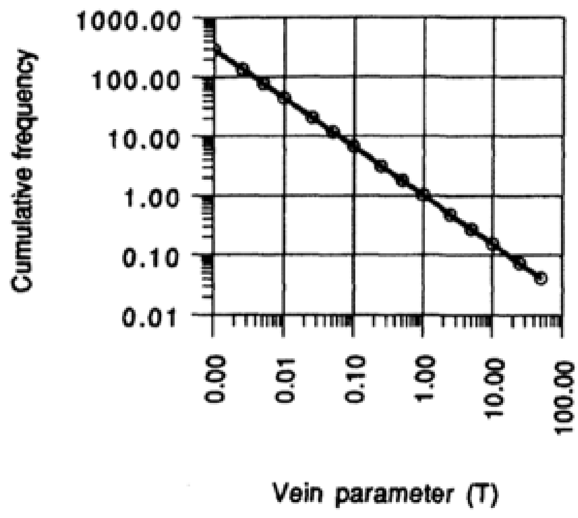

Figure 10. Power-law (fractal) distribution on a log-log cumulative frequency vs. vein/joint parameter, such as spacing. From McCaffrey et al., (1993).

Spacing distribution goodness-of-fit test

A power-law may not always be an appropriate model for fracture parameters (Bonnet et al., 2001) and so joint spacing distributions were also evaluated statistically—for composite datasets only—following a procedure adapted by Ehlen (1999). Stem-and-leaf plots were generated from the data which were then used to derive its frequency distribution. These distributions were then compared with lognormal, normal, gamma, and exponential distributions (see **Figure 11**) through the Chi-squared (χ^2) goodness-of-fit test at the 95% confidence level (Ehlen, 1999)(see **Appendix C**).

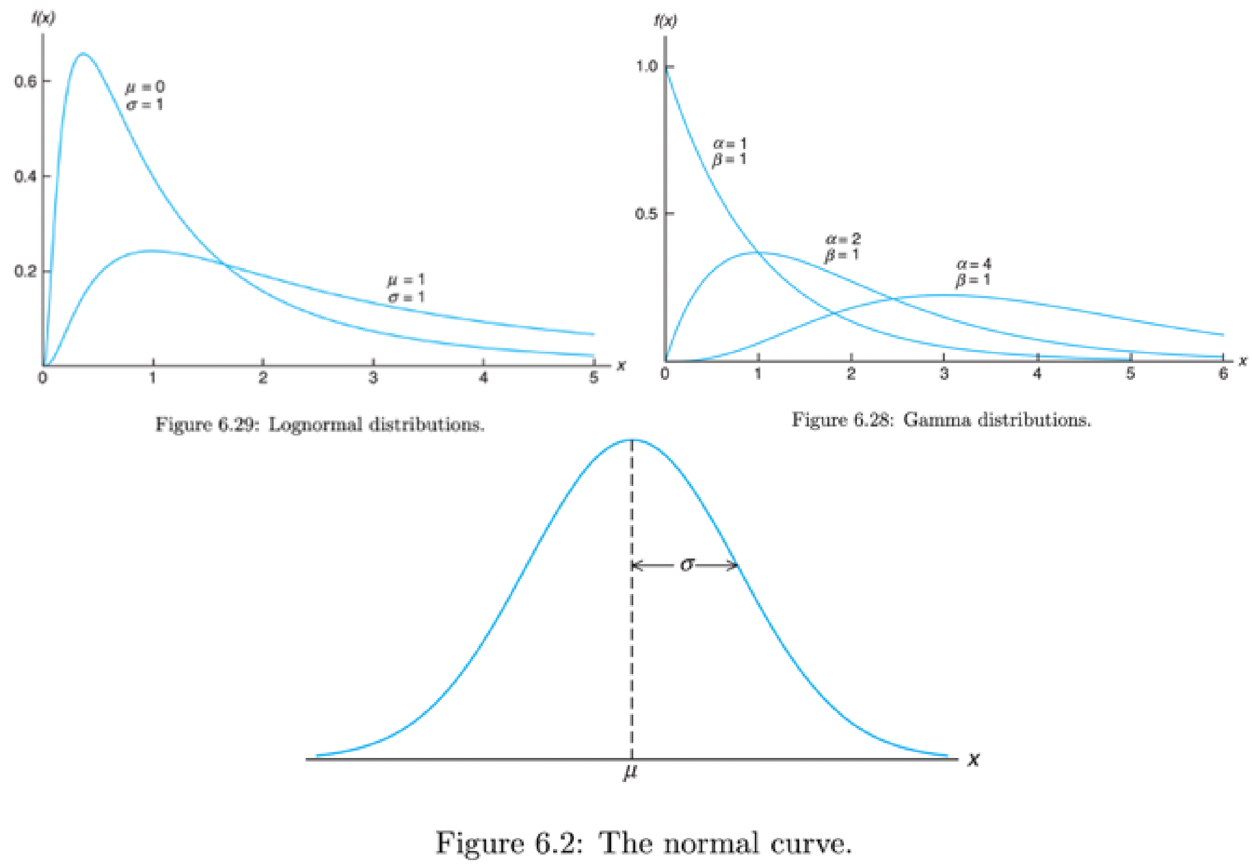

Figure 11. General form of lognormal, gamma (and exponential, $\alpha = 1$), and normal distributions. The tests performed do not assume the parameters shown (Walpole et al., 2012).

The null hypothesis (H_0) was either rejected if the test value χ^2 was greater than some critical value—exact value dependent on dataset and distribution tested against, see **Appendix A** and **C**—or rejected if otherwise (Walpole et al., 2012).

Kolmogorov-Smirnov tests for statistical similarity

Observed frequencies were also compared with the Kolmogorov-Smirnov (K-S) test (Ehlen, 1999). Since we assume the distributions to be highly skewed and we cannot assume that samples have been taken from a normal population (Walpole et al., 2012), the nonparametric test was employed (Ehlen, 1999). Nonetheless, this test allows us to identify significant similarities and differences in the joint spacing between the two preferred orientations by examining their relative cumulative frequency distributions under the null hypothesis that the datasets come from the same distribution (**Figure 12**).

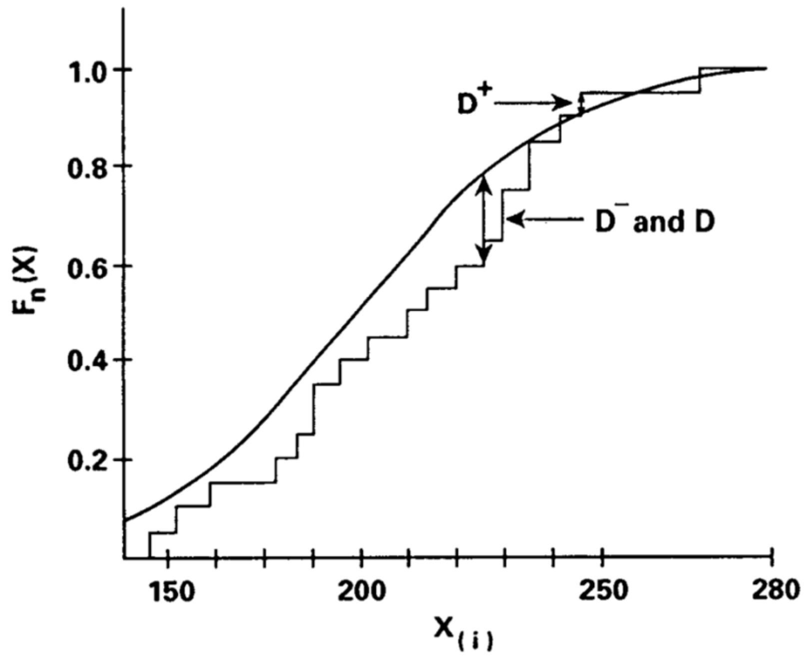

Figure 12. Example cumulative frequency distributions compared through the K-S statistic. From Boadu & Long, (1994).

Coefficient of variation

A final analysis used to characterize spacing was the coefficient of variation (c_v) which expresses the degree of clustering along a sample line (Gillespie et al., 2000). It can be calculated with,

$$c_v = \frac{\sigma}{\mu},$$

where σ and μ are the standard deviation and mean spacing of a dataset, respectively. Certain values are characteristic of specific distributions—$c_v = 1$ points toward a Poisson distribution—otherwise, $c_v > 1$ indicates clustering, and $c_v < 1$ indicates anti-clustering or regular spacing (Gillespie et al., 2000).

All the above analyses were then done for the Google Earth datasets with the exception that they were also compared to the corresponding field set through the K-S statistic.

RESULTS

General Statistics

Table 1: Dataset Statistics

Joint set	Mean strike (°)	Traverses	Segments	Data source	N	Spacing (cm)		
						Min	Max	Med.
1	150-330	4	17	F	292	1	1020	33
				GE	112	45	1073	183
2	66-246	4	23	F	275	1	1426	14
				GE	131	38	1887	210

Table 1 displays the general characteristics of our four datasets, each labeled either F or GE—corresponding to data source, the field or Google Earth—and in later tables with a 1 or 2—corresponding to the particular joint set, 2 being the master joints, 1 being the cross joints (according to recorded truncation data (Morse et al., 2020)). Here we summarize these results. Sample sizes along the same joint set between data sources are over 2.0 – 2.6 times higher in the field than Google Earth. Minimum calculated spacings were also smaller by 0.37 m to almost 0.5 m, while differences in maxima ranged almost an order of magnitude from 0.53 m to over 4.50 m. Measures of location such as median spacing were thus shifted to much larger values for GE datasets.

Calculated joint spacings in the field range over three orders of magnitude between 1 centimeter to 10s of meters within both sets. Those for the master set were notably larger than for the cross joints by about 4.0 m. Joint spacings from Google Earth ranged from 10s of centimeters to 10s of meters—highlighting this data source's previously mentioned disparity in the smaller sub-half-meter spacings.

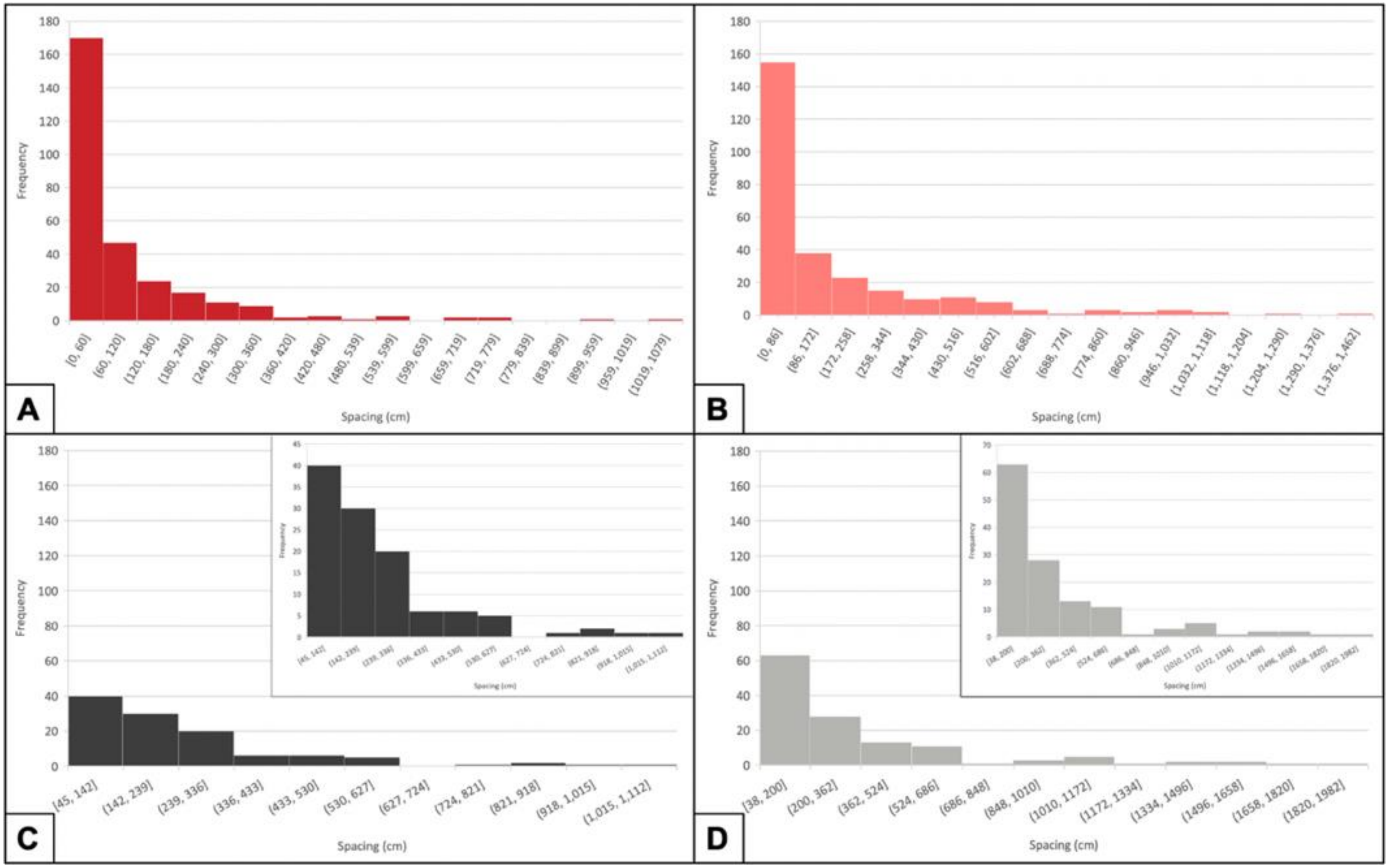

Figure 13. Joint spacing histograms of field data (**A.** joint set 1, **B.** joint set 2) and Google Earth data (**C.** joint set 1, **B.** joint set 2). **C.** and **D.** insets capture the structure of the Google Earth distributions hidden by the y-axis (frequency) range. (Each color used corresponds to that specific dataset in all of the following plots).

Frequency histograms of joint spacing indicate the data may be highly right skewed as expected for this kind of structure—though the inner structure of the first bin is mostly hidden from view and we cannot say for sure or discus modality. Still, bin 1 is much more pronounced for F data which again showcases the constraints of imagery resolution. Insets of **Figure 13C** and **D** show GE (Google Earth) histograms with a smaller y-axis range to show a more representative form of the distributions. Note the much higher frequencies in bins up to spacings of 500 to 600 cm. These are not encountered as often in the outcrop data where they are also especially dwarfed by measurements up to 60 – 86 cm.

Fractal Analysis

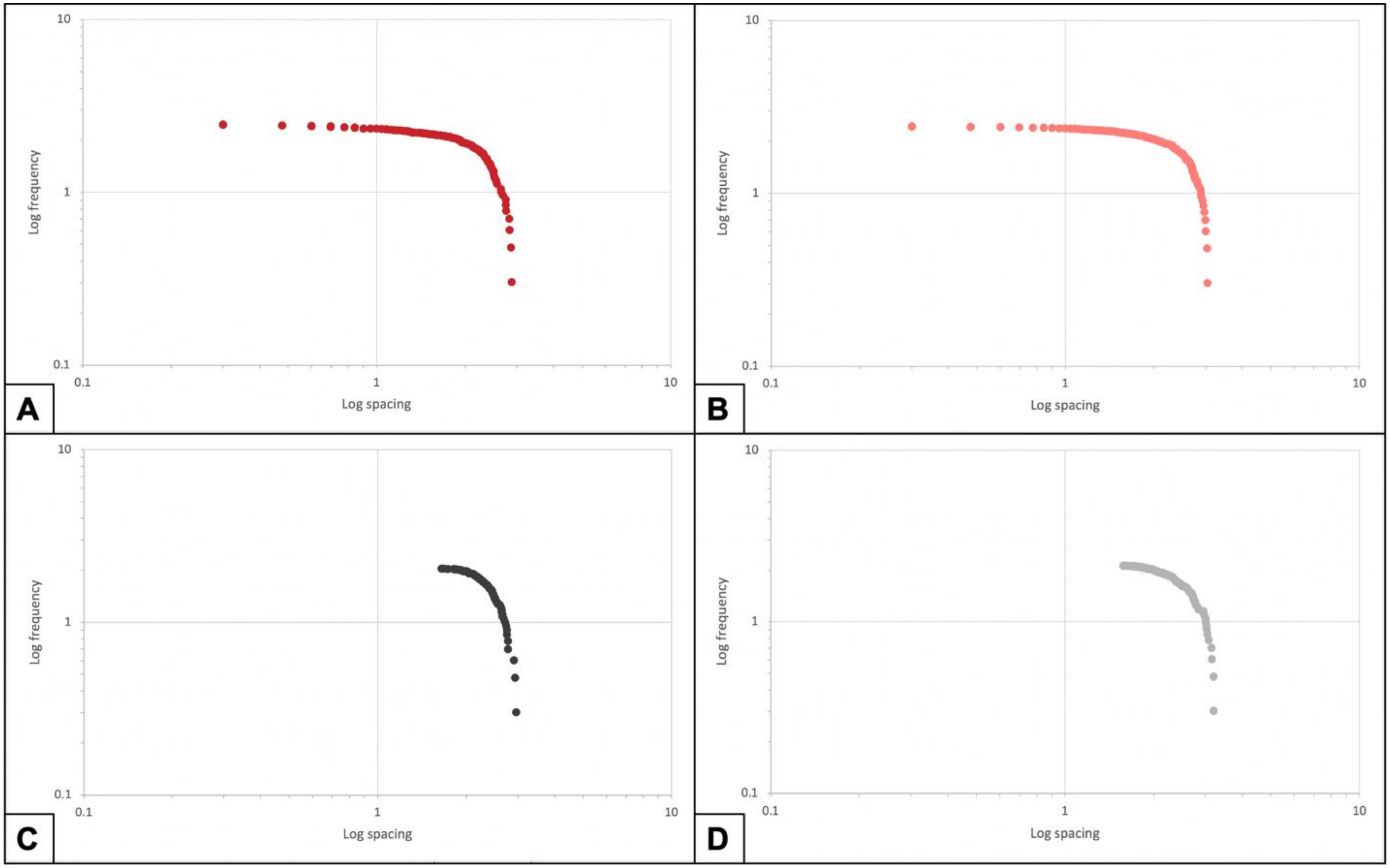

Figure 14. Log-log cumulative frequency vs. joint spacing plots of each dataset. **A.** F1. **B.** F2. **C.** GE1. **D.** GE2.

Generated log-log plots in **Figure 15** yield spacing distributions that can be characterized by generally smooth to somewhat sharp concave down curves, rather than a linear relationship; this holds true for all traverses on an individual basis as well as for the composite datasets shown above. Thus, our data does not reveal fractal behavior by this test, again, revealed by linearity (Bonnet et al., 2001; Ehlen, 2000; Le Garzic et al., 2011; McCaffrey et al., 1993). These curves also conveniently visualize sampling disparities at both the very small and very large spacings as data point density decreases substantially at both extremes. Along those lines, visual comparison between F and GE further highlights the lower limit problem of the imagery.

Goodness-of-Fit Tests

Table 2: Chi-Squared Goodness-of-fit Test Results (α = 0.05)

Joint set	Data source	Lognormal			Normal			Gamma			Exponential		
		Critical	Test	p	Critical	Test	p	Critical	Test	p	Critical	Test	p
1	F	15.507	11.533	0.17	14.067	57.357	~0	15.507	3.715	0.88	14.067	53.726	~0
	GE	15.507	3.068	0.93	15.507	42.281	~0	15.507	11.574	0.17	12.592	47.947	~0
2	F	19.675	15.957	0.14	21.026	84.534	~0	19.675	6.313	0.85	18.307	78.780	~0
	GE	19.675	22.199	0.02	19.675	126.594	~0	18.307	32.156	~0	18.307	32.652	~0

Chi-squared goodness-of-fit results in **Table 2** show both the critical and test values of each test along with their associated p-values. As a reminder, H_0 is rejected if the test value is greater than the critical and/or if the p-value is less than the level of significance, α. Our results indicate that the distributions for almost all datasets are either lognormal or gamma at the 0.05 confidence level—highlighted in green. Interestingly, we see that GE2 fails all tests. Note how close the critical and test values are for a lognormal distribution. Critical values vary naturally between test and dataset as a function of the given degrees of freedom of each frequency distributions (see **Appendix C1**). P-values show semi-consistent trends. All normal and exponential tests yield values of approximately zero. Field p-values are also quite similar, 0.17 and 0.14 for lognormal, and 0.88 and 0.85 for gamma, for F1 and F2, respectively. The highest p-value is associated with the lognormal test for GE1, 0.93.

Kolmogorov-Smirnov Tests

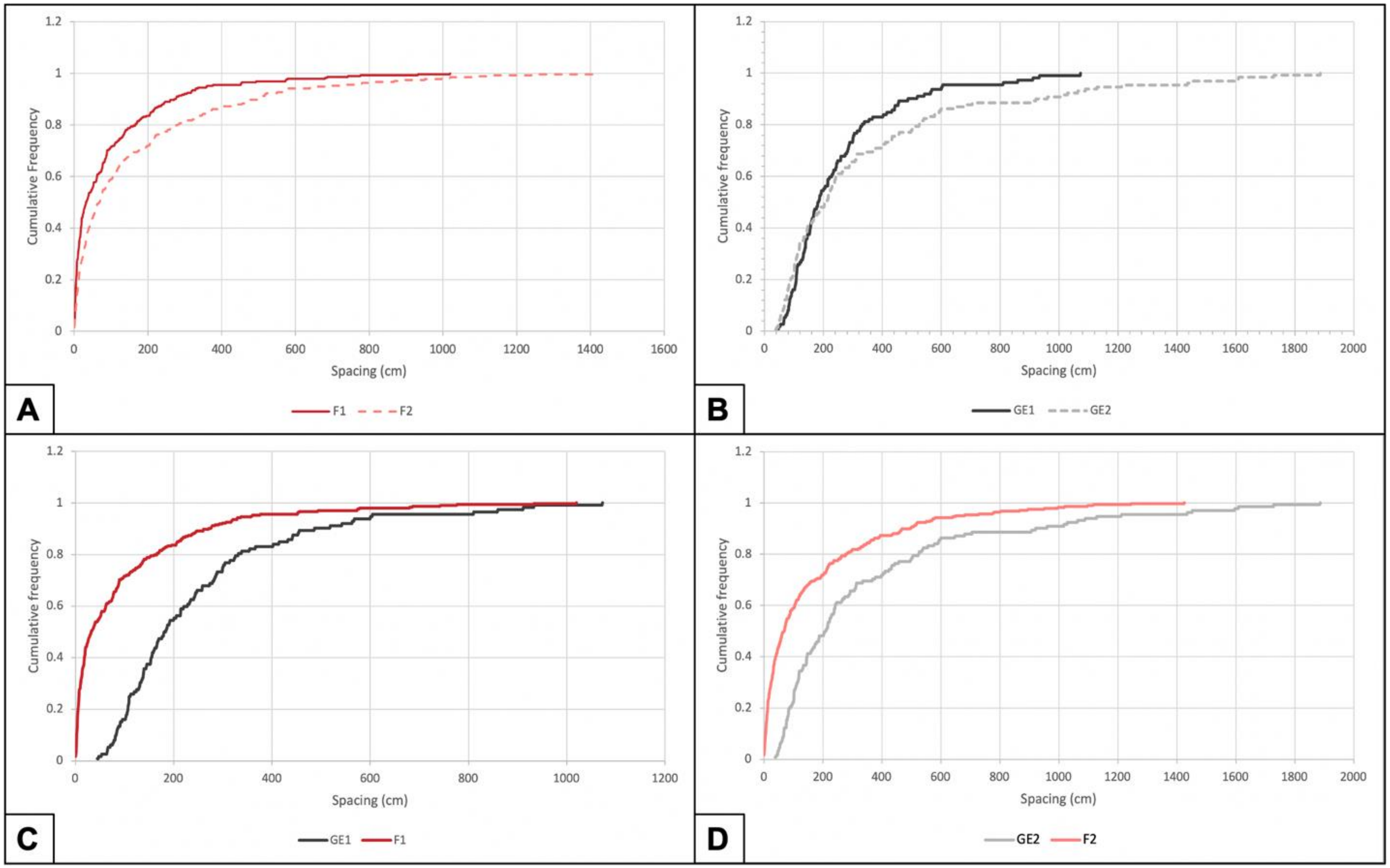

Figure 14. Cumulative frequency distribution comparisons used in the K-S test. **A.** F1-F2. **B.** GE1-GE2. **C.** F1-GE1. **D.** F2-GE2. (again, red: F1, light red: F2, dark gray: GE1, light gray: GE2. Curves dashed where similar colors are plotted together).

Table 3: Kolmogorov - Smirnov Test Results (α = 0.05)

Joint set	Comparison	Critical	Test	p
1	F1-F2	0.114	0.127	0.02
	GE1-GE2	0.175	0.117	0.38
2	F1-GE1	0.151	0.552	~0
	F2-GE2	0.145	0.406	~0

Figure 16 visually highlights the similarities between datasets at the same scale and the differences between those that were not. It should be noted that the *Cumulative frequency* plotted along the y-axis here is different than that in **Figure 15**. Here, the accumulation is through the relative frequency—taken as a portion or percentage of the sample size *N*—rather than whole number frequencies of encountering a certain value or less. **Table 3** displays our results for the K-S test itself. Again, we consider critical, test, and p-values.

Fig. 16A compares the master joints of set 2 and the cross joints of set 1. Set 2, wholly lying below set 1, can therefore be characterized by greater spacings, as discussed above. According to the K-S statistic we reject our null hypothesis that the datasets come from the same distribution. Still, note how close the test value is to the critical (0.127 vs. 0.114, respectively) and how close the p-value is to the level of significance (0.02 vs 0.05, respectively) (highlighted in yellow in **Table 3**). **Figure 16B** compares these two joint sets in Google Earth. Note their near identical behavior until about 150 cm (indicating the master joints to be less widely spaced than the cross joints) which then shifts to generally resemble the true relationship. This K-S test yields test and p-values (0.38) that indicate there is no statistical difference between the two datasets (highlighted in green in **Table 3**).

Figures 16C and **16D** compare data sources, F and GE, for joint sets 1 and 2, respectively. Here are the key differences. As expected, GE curves exhibit a much more rapid rise in cumulative frequency with greater spacing and even greater spacings than were reported in the field. Each curve also exhibits an inflection point within the first 200 centimeters, yet again highlighting the little role smaller spacings paly in their distributions. On the other hand, field data completely lack an inflection point. Resulting p-values were virtually zero indicating these distributions were distinctly statistically different.

Coefficient of Variation

Table 4: Coefficient of Variation

Dataset	Mean	St. Dev.	c_v
F1	99	152	1.54
F2	168	240	1.43
GE1	248	197	0.79
GE2	347	384	1.11

The coefficient of variation is a measure of clustering along sample lines (Gillespie et al., 2000). All datasets but GE1 were shown to exhibit clustering through its calculation (**Table 4**). In the field cross joints appeared clustered to a higher degree than the master joints by visual inspection. Their respective c_v appears to indicate that as well (1.54 vs. 1.43, respectively).

DISCUSSION

The range of our spacing data is somewhat close to that recorded by Martell et al. (1988) in the Mount Abbot Quadrangle in the central SNB. These went from a few 10s of centimeters to 10s of meters (Martel et al., 1988)—ours scaled an extra order of magnitude into the single digit centimeters. Joint spacing at our sites is also non-uniform—observed in other granitic rocks such as the Florence Lake Mount Givens granodiorite, also of the central SNB (Segall & Pollard, 1983)—in contrast to the more regular spacing of cross joints in sedimentary layers (Ruf et al., 1997).

Measurement Uncertainty

As measurements were taken in the field it is appropriate to address their uncertainty. Each position recorded can be considered accurate with a standard uncertainty of 0.005 cm—half the smallest tick mark on our tape (one mm). Even if we were to determine the resulting uncertainty of our spacings through propagation of errors with standard deviations $\left(\Delta s = \sqrt{\Delta p_j^2 + \Delta p_i^2}\right)$–the Δ here signifying uncertainty—the result would be similarly small; however, our data is not error free. On one hand, the use of a one-dimensional traverse may introduce a sampling bias which can be significant where strikes vary from perfectly orthogonal to the traverse (Ryan, 2000; Sousa, 2010). As previously mentioned, we worked with a cutoff of around 5°-10° from perpendicular to allow for variations in individual joint strikes. This may be overcome with a simple geometric correction which considers the angle between a joint and the normal to the traverse enabling us to calculate the true spacing (Ryan, 2000; McCaffrey et al., 1993).

There were also many instances where measurements required a projection from the outcrop to the traverse. In one situation the measuring tape did not lay perfectly flat on the portion of the outcrop being sampled. This was largely due to the weathering and erosion of blocks downslope. We were then required to project our measurements from the traverse to the joints underneath. Similarly, if sampling through a section of regolith or vegetative cover, lateral projections were made in a similar manner. Measurements recorded in this fashion may have an uncertainty of up to a few centimeters, depending on the distance of the projection, and may have included significant errors, especially effecting our representation of the smaller spacings. Traverse locations were chosen in an attempt to maximize length and therefore did not wholly consider these limitations. A more refined criteria for traverse location that explicitly attempts to maximize length and minimize the need for projections could be employed to minimize these effects. Also, similar measurements can be made to establish a vertical correction to the horizontal to model "flatness" in relation to the outcrop.

Are the Spacing Distributions Fractal?

A power-law may be assumed to model the spacing distribution of a joint population when its trend on a log-log cumulative frequency vs. spacing plot can approximate a straight line (Bonnet et al., 2001; McCaffrey et al., 1993). Our datasets lack this behavior and instead resemble data collected by McCaffrey et al. (1993) in the County Galway Granite at Mace Head, Ireland (**Figure 17**).

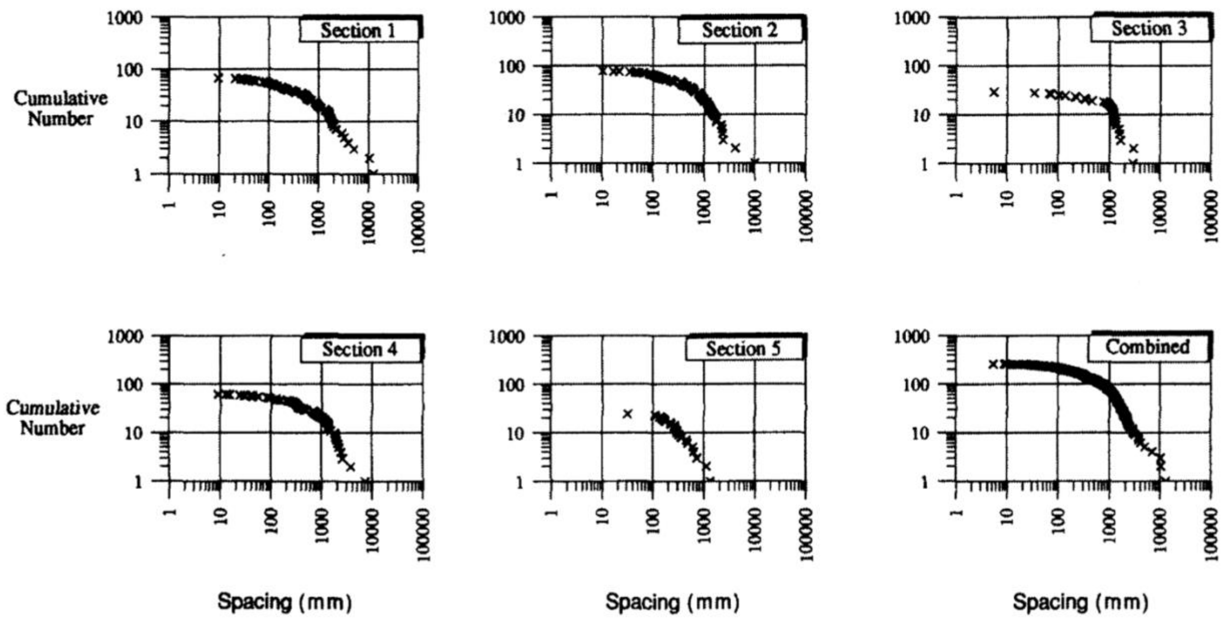

Figure 15. Log-log cumulative frequency vs. vein spacing plots for individual datasets and a composite (McCaffrey et al., 1993).

This has been shown to be typical of the negative exponential and lognormal distributions (McCaffrey et al., 1993). Further tests carried out by McCaffrey et al. (1993) agree and a linear regression analysis yielded an R^2 of 96-99.1% for a lognormal distribution and only 60-82% for an exponential. Lognormal and exponential distributions (Clark et al., 1995; McCaffrey et al., 1993; Wong et al., 2018) are also commonly seen in the literature to describe joint spacing (Le Garzic et al., 2011; Sousa, 2010). Lognormal is perhaps the most frequently reported (Palmström, 1995) and has been observed in other granites such as in Stripa, Sweden by Roleau and Gale (1985). Our goodness-of-fit results seem to generally agree with these findings except that our distributions are best fit by a lognormal and gamma—exponential is in fact a subset of the gamma distribution (Walpole et al., 2012).

These results may represent the true distribution or simply further sampling biases at the small and large scales called truncation and censoring, respectively (Bertrand et al., 2015; Bonnet et al., 2001; Le Garzic et al., 2011). In most cases, these biases may cause deviations on the experimental log-log plot from linearity for power-law distributions (Bonnet et al., 2001). An under sampling of the smallest spacings is typically due to the resolution of the sampling technique used, while an underestimation of the largest may be due to the finite size of the sample domain and the lower probability of encountering larger size population values (Bonnet et al., 2001; Le Garzic et al., 2011). Most authors have simply truncated their own data to stem the former, effectively removing the part of their distribution believed to be biased. Unfortunately, there is not an established standard for this threshold and most researchers subjectively fix it below the point which they believe joints to be incompletely recorded. Spacing values less than the mode of a distribution are generally considered to be incompletely sampled so this could be an appropriate cutoff. Though sampling resolution is thought to be the primary cause of deviation from a power-law trend at small scales other mechanism have been suggested. One is the existence of a physical lower limit to power-law size populations such as 1 m for length distributions. All power laws in nature must have these lower and upper cutoffs. The generally accepted range of values for a robust characterization of a power-law distribution is 2-3 orders of magnitude (Bonnet et al., 2001). We achieved this with our opportunistic traverse locations and lengths but perhaps extending our measurements and measurement accuracy into the millimeters may yield more representative results (McCaffrey et al., 1993).

Given these, and other, sampling biases, many different distributions such as the power-law have been shown to produce samples that are approximately lognormal (Bonnet et al., 2001; Palmström, 1995) and even gamma under the appropriate conditions (Bonnet et al., 2001). Analog experiments by Reches (1986) of fracture system development have also shown that there exists a transition between power-law and lognormal size distributions with increased deformation indicating that distributions may change with time and that a power-laws could help identify young populations (Bonnet et al., 2001). Rives et al. (1992) even found that two-dimensional trace lengths were best described as lognormal in sample but as a population were power-law (Ehlen, 2000). Clearly, a rigorous sampling scheme from the smallest to the largest scales is required to appropriately test fractal geometries (McCaffrey et al., 1993). An added suggestion is to apply the goodness-of-fit test directly to a power-law distribution. This was not considered for this paper as it requires parameter estimation procedures that are outside the present capabilities of the author. Still, a maximum likelihood estimation could be applied to not only determine power-law parameters but more explicitly those for the gamma, exponential, and even Weibull distributions (not tested in this paper). Similarly, the estimation of the probability of making Type I (rejecting H_0 when true) and Type II (accepting H_0 when false) errors and linear regression analyses for correlation should be considered (Walpole et al., 2012).

Lastly, Ehlen (1999) recommends a minimum number of spacing measurements to acquire a stable fractal dimension that is based on the nature of the sampled joint pattern itself. We chose a target of 100-150 per traverse, however, this is best applied to regularly spaced joints, while 200 or more spacings are required for a non-uniform or irregular spacing such as at our sites (Ehlen, 2000). As previously mentioned, no traverse surpassed these thresholds, but our composite datasets have substantially—292 and 275—and it remains unclear whether a fractal dimension may have stabilized or not. Therefore, as another check on fractal behavior, future studies should determine whether that stability was reached.

Now, the reason for such a wide variety of statistical joint spacing distribution models is still unclear (Wong et al., 2018); however, there are some suggestions. As with the power-law, an assortment of distributions may characterize different stages of fracture pattern development (Ehlen, 2000). This could be extremely useful in determining the progression of deformation events related to fracturing and further corroborate age relationships between fracture patterns. Also, lognormal distributions may characterize an upper limit of joint density—saturation threshold—in granites where progressive joint development effectively ceases (Wong et al., 2018). It has also been suggested that distributions may be related to the mode of fracturing and the initial stress conditions (Boadu & Long, 1994). These suggestions largely pose questions about the evolution of a joint system which may be best explored through numerical modeling. Not a lot of fracture spacing work has been done with computational methods (Wong et al., 2018) but the ability to control material parameters, boundary conditions, and the laws of physics, may provide invaluable insight on the key elements of joint development (Fossen, 2016).

How do the Spacing Distributions Compare?

Preliminary results ignited an interest to directly compare the spacing distributions of our two joint sets statistically which could reveal something about the joined fracture forming histories of these two sets, and the nature of spacing in relation to that history. The K-S test between the master and cross joints led to a rejection of our null hypothesis that the distributions are the same (**Table 3**). This is to be expected for different joint sets—even within the same rock unit (Pollard & Aydin, 1988)—especially ones with such consistent truncation relationships (Morse et al., 2020). We also notice distinct differences between them such as generally larger spacings within the master set (**Figure 16A**) and a lesser degree of clustering (**Table 4**); however, the grounds for rejection are quite equivocal. The critical region was any value greater than 0.114. Our test value was only 0.127, only crossing that threshold by 0.013. Similarly, our p-value was quite close to the level of significance (0.02 vs. 0.05, respectively). Therefore, we are unable to infer the likely reality from these results (Walpole et al., 2012). It is likely that many of the previous recommendations to achieve even more representative datasets could overcome this and provide a more distinct outcome. When comparing joint spacing distributions, it may also be of interest to plot their respective relative cumulative frequency distributions (**Figure** 16) whether or not the K-S test will be performed to effectively visualize their differences and similarities.

Also, where consistent age relationships are observed, it would be of interest to measure the possible influence of the spacing of the arresting set on the spacing of the arrested set. It has been shown that discontinuities themselves affect the growth of other joints and that their spacing may act as an effective mechanical layering in sedimentary beds (Ruf et al., 1997). Investigations of this sort in igneous rocks may yield interesting relationships and assist with our characterization of joint patterns.

Can Google Earth Datasets Yield Representative Joint Spacing Distributions?

Lastly, we will discuss the utilization of Google Earth in fracture analysis—namely for joint spacing. Each analysis carried out in this paper highlights the underestimation of joint spacings in datasets collected through Google Earth Imagery (see **Figures 13, 14,** and **15**)—no spacings were recorded below 0.38 m. It is not surprising that K-S results show them to be statistically different than their counterpart field dataset. These results are unequivocal, unlike the previous, as test values were much larger than critical, and p-values are virtually zeros (Walpole et al., 2012). Still, distribution form seems somewhat preserved, through visual inspection of spacing histograms (**Figure** 13) and statistically, as GE1 was best fit by a lognormal distribution with the highest p-value of any test, 0.93. Position descriptors are not maintained however, as the underestimation of smaller spacings has led to the artificial generation of larger spacings and have shifted the distribution. Google Earth is still of great scientific value and If used for spacing analyses the above constraints must be considered. The comparison of field datasets and those collected in Google Earth should be continued for refined quantitative measures of resolution bias and accuracy.

What is somewhat surprising is how similar Google Earth datasets 1 and 2 are to each other. They are the only datasets which pass the K-S test—and quite significantly with a p-value of 0.38. As, mentioned this is likely attributed to the significant overlap between the two destructions at the smaller spacings recorded. This may be an expression of the lower limits of the imagery's resolution. Both sets were sampled from the same images and we may therefore miss the same size joints. We cannot be exactly sure as Google Earth remains a black box with very limited public documentation on its inner workings (Fisher et al., 2012).

CONCLUSIONS

We investigate two sub-orthogonal joint sets in the Sierra Nevada Batholith, California, to, 1) characterize their spacing distributions with an interest in fractal behavior, 2) directly compare the spacing distributions of these sets of apparent different ages, and 3) determine whether Google Earth can yield representative datasets for joint spacing analyses.

The spacing distributions for master and cross joint datasets are best described by lognormal or gamma and not power-law (fractal) at the 0.05 significance level. This result may also reflect the true distribution or sampling biases such as truncation or censoring of which the fractal signature is sensitive too (Bertrand et al., 2015; Bonnet et al., 2001; Le Garzic et al., 2011). This may be overcome with even greater sample sizes and also by extending the lower limit of measurements another order of magnitude into the millimeters (Bonnet et al., 2001). Other analyses should also be performed alongside the log-log fractal test plot for a more robust determination of fractal behavior such as a fractal dimension stability analysis (Ehlen, 2000) and directly testing the fit of a power-law distribution.

As expected, the spacing of the older master joints and younger cross joints are different—the former exhibits a consistently greater frequency of wider spacings and lesser degree of clustering. The statistical difference is still unclear as K-S test and critical values are remarkably close. The previous recommendations related to sampling scheme would likely overcome this result. The relationship between the spacing of these two sets should also be explored further to determine whether arresting joints within igneous rocks may also define a mechanical layer thickness and therefore constrain the spacing of arrested joints (Ruf et al., 1997).

All analyses highlight departures from reality when comparing datasets collected in field outcrops and on Google Earth imagery. The latter consistently misses the smallest spacings and as a result generates artificially large spacings. They are shown to somewhat preserve distribution form (e.g., lognormality) but then shift their position towards larger values. Google Earth spacing distributions were then distinctly statistically different than field spacing distributions. Therefore, datasets from Google Earth cannot be analyzed under the assumption that they represent the true spacing distribution of a joint set. Ultimately, within fracture analysis, Google Earth can only be fully utilized as a field site reconnaissance and mapping tool, and any analyses done through it should be corroborated with field work.

APPENDIX

Appendix A – Data

Table A1: Field Dataset 1

Site	Traverse	Joint number	Position (m)	Position (cm)	Spacing (cm)	Site	Traverse	Joint number	Position (m)	Position (cm)	Spacing (cm)	Site	Traverse	Joint number	Position (m)	Position (cm)	Spacing (cm)	Site	Traverse	Joint number	Position (m)	Position (cm)	Spacing (cm)
1.3	1	**1**	1.30	130	130	1.3	1	**74**	4.18	418	99	1.3	5	**147**	6.42	642	18	2.4	1	**220**	11.04	1104	3
		2	3.60	360	230			**75**	4.37	437	19			**148**	6.44	644	2			**221**	11.14	1114	10
		3	3.75	375	15			**76**	4.62	462	25			**149**	6.46	646	2			**222**	11.17	1117	3
		4	3.80	380	5			**77**	4.69	469	7			**150**	6.65	665	19			**223**	11.18	1118	1
		5	4.32	432	52			**78**	5.18	518	49			**151**	8.44	844	179			**224**	11.27	1127	9
		6	5.45	545	113			**79**	6.85	685	167			**152**	11.74	1174	330			**225**	11.45	1145	18
		7	8.06	806	261			**80**	0.90	90	90			**153**	11.86	1186	12			**226**	11.59	1159	14
		8	10.49	1049	243			**81**	3.06	306	216			**154**	13.23	1323	137			**227**	11.67	1167	8
		9	10.70	1070	21			**82**	3.83	383	77			**155**	14.00	1400	77			**228**	11.73	1173	6
		10	11.08	1108	38			**83**	9.58	958	575			**156**	14.30	1430	30			**229**	12.34	1234	61
		11	11.70	1170	62			**84**	10.20	1020	62			**157**	14.36	1436	6			**230**	12.45	1245	11
		12	11.91	1191	21			**85**	0.51	51	51			**158**	14.73	1473	37			**231**	12.50	1250	5
		13	12.02	1202	11			**86**	0.67	67	16			**159**	14.80	1480	7			**232**	13.00	1300	50
		14	12.10	1210	8			**87**	0.88	88	21			**160**	14.91	1491	11			**233**	16.00	1600	300
		15	12.18	1218	8			**88**	1.56	156	68			**161**	2.77	277	277			**234**	19.61	1961	361
		16	12.94	1294	76			**89**	1.70	170	14			**162**	3.40	340	63			**235**	1.09	109	109
		17	13.12	1312	18			**90**	3.54	354	184			**163**	7.17	717	377			**236**	2.28	228	119
		18	14.52	1452	140			**91**	3.85	385	31			**164**	12.11	1211	494			**237**	3.00	300	72
		19	15.05	1505	53	1.3	3	**92**	1.04	104	104			**165**	13.21	1321	110			**238**	3.54	354	54
		20	15.10	1510	5			**93**	3.82	382	278			**166**	13.90	1390	69			**239**	6.15	615	261
		21	15.37	1537	27			**94**	3.97	397	15			**167**	14.68	1468	78			**240**	11.89	1189	574
		22	15.63	1563	26			**95**	4.06	406	9			**168**	14.73	1473	5			**241**	13.85	1385	196
		23	18.01	1801	238			**96**	4.09	409	3			**169**	14.80	1480	7			**242**	15.30	1530	145
		24	18.31	1831	30			**97**	4.13	413	4			**170**	14.87	1487	7			**243**	6.81	681	681
		25	19.97	1997	166			**98**	4.17	417	4			**171**	14.89	1489	2			**244**	6.82	682	1
		26	20.29	2029	32			**99**	4.20	420	3			**172**	15.64	1564	75			**245**	7.68	768	86
		27	21.18	2118	89			**100**	4.25	425	5			**173**	15.70	1570	6			**246**	8.43	843	75
		28	23.06	2306	188			**101**	4.28	428	3			**174**	15.76	1576	6			**247**	8.62	862	19
		29	23.14	2314	8			**102**	4.55	455	27			**175**	15.81	1581	5			**248**	8.69	869	7
		30	23.20	2320	6			**103**	4.60	460	5			**176**	15.86	1586	5			**249**	9.16	916	47
		31	23.23	2323	3			**104**	4.64	464	4			**177**	16.73	1673	87			**250**	9.19	919	3
		32	24.23	2423	100			**105**	4.84	484	20			**178**	23.60	2360	687			**251**	9.26	926	7
		33	0.27	27	27			**106**	5.63	563	79			**179**	25.66	2566	206			**252**	9.32	932	6
		34	0.91	91	64			**107**	7.34	734	171			**180**	4.53	453	453			**253**	9.35	935	3
		35	6.70	670	579			**108**	8.71	871	137			**181**	7.90	790	337			**254**	9.41	941	6
		36	6.74	674	4			**109**	9.25	925	54			**182**	9.23	923	133			**255**	9.45	945	4
		37	6.77	677	3			**110**	10.60	1060	135			**183**	9.56	956	33			**256**	9.53	953	8
		38	7.71	771	94	1.3	5	**111**	0.14	14	14			**184**	14.09	1409	453			**257**	9.57	957	4
		39	7.83	783	12			**112**	0.18	18	4			**185**	14.12	1412	3			**258**	9.65	965	8
		40	17.16	1716	933			**113**	1.64	164	146			**186**	14.90	1490	78			**259**	9.89	989	24
		41	18.13	1813	97			**114**	1.72	172	8			**187**	15.30	1530	40			**260**	9.92	992	3
		42	19.03	1903	90			**115**	1.77	177	5			**188**	15.49	1549	19			**261**	9.96	996	4
		43	19.15	1915	12			**116**	3.31	331	154			**189**	17.60	1760	211			**262**	9.97	997	1
		44	20.02	2002	87			**117**	6.10	610	279			**190**	18.44	1844	84			**263**	10.01	1001	4
		45	23.61	2361	359			**118**	8.95	895	285			**191**	18.45	1845	1			**264**	10.03	1003	2
		46	23.74	2374	13			**119**	10.12	1012	117			**192**	20.52	2052	207			**265**	10.10	1010	7
		47	24.58	2458	84			**120**	10.95	1095	83			**193**	20.88	2088	36			**266**	10.11	1011	1
		48	27.65	2765	307			**121**	18.38	1838	743			**194**	20.91	2091	3			**267**	10.16	1016	5
		49	27.82	2782	17			**122**	20.83	2083	245			**195**	21.32	2132	41			**268**	10.30	1030	14
		50	27.84	2784	2			**123**	22.20	2220	137			**196**	21.35	2135	3			**269**	10.43	1043	13
		51	0.53	53	53			**124**	24.28	2428	208			**197**	21.39	2139	4			**270**	10.61	1061	18
		52	0.61	61	8			**125**	26.65	2665	237			**198**	21.42	2142	3			**271**	10.63	1063	2
		53	0.82	82	21			**126**	27.10	2710	45			**199**	21.58	2158	16			**272**	10.96	1096	33
		54	5.38	538	456			**127**	28.82	2882	172			**200**	21.86	2186	28			**273**	10.99	1099	3
		55	6.26	626	88			**128**	1.23	123	123			**201**	22.39	2239	53			**274**	12.22	1222	123
		56	8.72	872	246			**129**	2.12	212	89			**202**	25.57	2557	318			**275**	12.51	1251	29
		57	9.99	999	127			**130**	2.16	216	4			**203**	25.90	2590	33			**276**	14.70	1470	219
		58	10.14	1014	15			**131**	2.23	223	7	2.4	1	**204**	3.30	330	330			**277**	1.33	133	133
		59	10.28	1028	14			**132**	2.64	264	41			**205**	4.08	408	78			**278**	1.93	193	60
		60	10.42	1042	14			**133**	3.04	304	40			**206**	4.87	487	79			**279**	4.18	418	225
		61	10.47	1047	5			**134**	3.23	323	19			**207**	6.27	627	140			**280**	4.36	436	18
		62	10.50	1050	3			**135**	3.31	331	8			**208**	14.04	1404	777			**281**	6.18	618	182
		63	10.58	1058	8			**136**	3.66	366	35			**209**	14.42	1442	38			**282**	9.39	939	321
		64	10.70	1070	12			**137**	3.78	378	12			**210**	15.54	1554	112			**283**	11.00	1100	161
		65	11.52	1152	82			**138**	4.04	404	26			**211**	15.78	1578	24			**284**	11.90	1190	90
		66	2.72	272	272			**139**	4.67	467	63			**212**	16.41	1641	63			**285**	14.10	1410	220
		67	5.65	565	293			**140**	4.78	478	11			**213**	10.20	1020	1020			**286**	15.62	1562	152
		68	6.12	612	47			**141**	4.99	499	21			**214**	10.39	1039	19			**287**	17.67	1767	205
		69	6.18	618	6			**142**	5.20	520	21			**215**	10.54	1054	15			**288**	19.83	1983	216
		70	6.38	638	20			**143**	5.81	581	61			**216**	10.72	1072	18			**289**	20.72	2072	89
		71	6.77	677	39			**144**	5.92	592	11			**217**	10.74	1074	2			**290**	20.94	2094	22
		72	8.54	854	177			**145**	6.16	616	24			**218**	10.95	1095	21			**291**	20.98	2098	4
		73	3.19	319	319			**146**	6.24	624	8			**219**	11.01	1101	6			**292**	22.70	2270	172

Table A2: Field Dataset 2

Site	Traverse	Number	Position (m)	Position (cm)	Spacing (cm)
1.3	2	**1**	0.76	76	76
		2	1.51	151	75
		3	3.50	350	199
		4	4.06	406	56
		5	4.98	498	92
		6	5.82	582	84
		7	6.40	640	58
		8	6.69	669	29
		9	7.02	702	33
		10	7.07	707	5
		11	7.18	718	11
		12	7.26	726	8
		13	11.88	1188	462
		14	11.90	1190	2
		15	12.03	1203	13
		16	12.15	1215	12
		17	12.39	1239	24
		18	12.71	1271	32
		19	12.88	1288	17
		20	13.00	1300	12
		21	14.05	1405	105
		22	14.14	1414	9
		23	15.10	1510	96
		24	15.62	1562	52
		25	16.14	1614	52
		26	16.30	1630	16
		27	16.64	1664	34
		28	16.97	1697	33
		29	17.66	1766	69
		30	18.28	1828	62
		31	18.37	1837	9
		32	19.40	1940	103
		33	19.60	1960	20
		34	21.95	2195	235
		35	25.70	2570	375
		36	0.36	36	36
		37	4.75	475	439
		38	5.98	598	123
		39	8.75	875	277
		40	13.31	1331	456
		41	13.40	1340	9
		42	13.68	1368	28
		43	20.97	2097	729
		44	21.46	2146	49
		45	26.54	2654	508
		46	28.65	2865	211
		47	28.79	2879	14
		48	29.20	2920	41
		49	0.47	47	47
		50	0.54	54	7
		51	1.26	126	72
		52	1.44	144	18
		53	2.34	234	90
		54	2.80	280	46
		55	7.15	715	435
		56	7.28	728	13
		57	8.63	863	135
		58	9.34	934	71
		59	12.17	1217	283
		60	13.93	1393	176
		61	17.30	1730	337
		62	18.01	1801	71
		63	20.22	2022	221
		64	20.37	2037	15
		65	20.65	2065	28
		66	20.85	2085	20
		67	21.25	2125	40
		68	22.30	2230	105
		69	0.40	40	40
1.3	2	**70**	1.26	126	86
		71	2.54	254	128
		72	2.62	262	8
		73	2.76	276	14
		74	3.34	334	58
		75	3.70	370	36
		76	4.09	409	39
		77	4.84	484	75
		78	8.30	830	346
		79	8.66	866	36
		80	11.30	1130	264
		81	11.65	1165	35
		82	12.63	1263	98
1.3	4	**83**	1.48	148	148
		84	1.59	159	11
		85	1.84	184	25
		86	2.44	244	60
		87	2.76	276	32
		88	2.87	287	11
		89	7.55	755	468
		90	13.06	1306	551
		91	13.43	1343	37
		92	13.73	1373	30
		93	14.91	1491	118
		94	15.35	1535	44
		95	15.36	1536	1
		96	15.38	1538	2
		97	15.48	1548	10
		98	19.21	1921	373
		99	20.76	2076	155
		100	21.81	2181	105
		101	25.76	2576	395
		102	3.50	350	350
		103	4.71	471	121
		104	6.64	664	193
		105	12.45	1245	581
		106	20.48	2048	803
		107	23.88	2388	340
		108	27.52	2752	364
		109	0.63	63	63
		110	0.75	75	12
		111	3.69	369	294
		112	4.15	415	46
		113	12.83	1283	868
		114	15.44	1544	261
		115	18.21	1821	277
		116	18.53	1853	32
		117	18.67	1867	14
		118	18.77	1877	10
		119	22.05	2205	328
		120	27.27	2727	522
		121	27.85	2785	58
		122	9.51	951	951
		123	9.65	965	14
		124	9.96	996	31
		125	15.08	1508	512
		126	15.42	1542	34
		127	29.68	2968	1426
1.4	2	**128**	11.18	1118	1118
		129	11.91	1191	73
		130	15.50	1550	359
		131	17.07	1707	157
		132	19.23	1923	216
		133	21.60	2160	237
		134	27.32	2732	572
		135	0.47	47	47
		136	1.89	189	142
		137	3.25	325	136
		138	9.75	975	650
1.4	2	**139**	14.38	1438	463
		140	20.03	2003	565
		141	12.45	1245	1245
		142	11.95	1295	50
		143	16.85	1685	390
		144	19.22	1922	237
		145	20.00	2000	78
		146	29.97	2997	997
		147	5.00	500	500
		148	9.98	998	498
		149	17.79	1779	781
		150	19.91	1991	212
		151	22.05	2205	214
		152	2.13	213	213
		153	2.42	242	29
		154	13.40	1340	1098
		155	22.36	2236	896
		156	23.62	2362	126
		157	24.49	2449	87
		158	25.56	2556	107
		159	28.10	2810	254
		160	28.35	2835	25
		161	29.45	2945	110
		162	29.60	2960	15
		163	30.03	3003	43
		164	3.00	300	300
		165	5.53	553	253
		166	9.46	946	393
		167	11.40	1140	194
		168	0.23	23	23
		169	2.28	228	205
		170	7.46	746	518
		171	8.17	817	71
		172	8.60	860	43
		173	13.78	1378	518
		174	14.68	1468	90
		175	0.27	27	27
		176	0.81	81	54
		177	2.12	212	131
		178	2.79	279	67
		179	2.93	293	14
		180	4.11	411	118
		181	5.19	519	108
		182	5.45	545	26
		183	5.78	578	33
		184	8.64	864	286
		185	13.30	1330	466
		186	19.70	1970	640
2.4	1	**187**	3.30	330	330
		188	4.08	408	78
		189	4.87	487	79
		190	6.27	627	140
		191	14.04	1404	777
		192	14.42	1442	38
		193	15.54	1554	112
		194	15.78	1578	24
		195	16.41	1641	63
		196	10.20	1020	1020
		197	10.39	1039	19
		198	10.54	1054	15
		199	10.72	1072	18
		200	10.74	1074	2
		201	10.95	1095	21
		202	11.01	1101	6
		203	11.04	1104	3
		204	11.14	1114	10
		205	11.17	1117	3
		206	11.18	1118	1
		207	11.27	1127	9
2.4	1	**208**	11.45	1145	18
		209	11.59	1159	14
		210	11.67	1167	8
		211	11.73	1173	6
		212	12.34	1234	61
		213	12.45	1245	11
		214	12.50	1250	5
		215	13.06	1306	56
		216	16.06	1606	300
		217	19.67	1967	361
		218	1.09	109	109
		219	2.28	228	119
		220	3.00	300	72
		221	3.54	354	54
		222	6.15	615	261
		223	11.89	1189	574
		224	13.85	1385	196
		225	15.30	1530	145
		226	6.81	681	681
		227	6.82	682	1
		228	7.68	768	86
		229	8.43	843	75
		230	8.62	862	19
		231	8.69	869	7
		232	9.16	916	47
		233	9.19	919	3
		234	9.26	926	7
		235	9.32	932	6
		236	9.35	935	3
		237	9.41	941	6
		238	9.45	945	4
		239	9.53	953	8
		240	9.57	957	4
		241	9.65	965	8
		242	9.89	989	24
		243	9.92	992	3
		244	9.96	996	4
		245	9.97	997	1
		246	10.01	1001	4
		247	10.03	1003	2
		248	10.10	1010	7
		249	10.11	1011	1
		250	10.16	1016	5
		251	10.30	1030	14
		252	10.43	1043	13
		253	10.61	1061	18
		254	10.63	1063	2
		255	10.96	1096	33
		256	10.99	1099	3
		257	12.22	1222	123
		258	12.51	1251	29
		259	14.70	1470	219
		260	1.33	133	133
		261	1.93	193	60
		262	4.18	418	225
		263	4.36	436	18
		264	6.18	618	182
		265	9.39	939	321
		266	11.00	1100	161
		267	11.90	1190	90
		268	14.10	1410	220
		269	15.62	1562	152
		270	17.67	1767	205
		271	19.83	1983	216
		272	20.72	2072	89
		273	20.94	2094	22
		274	20.98	2098	4
		275	22.70	2270	172

Table A3: F1 strikes and dips

Site	Traverse	Segment	Strike (°)	Strike - 180 (°)	Corrected (°)	Corrected - 180 (°)	Dip (°)
1.3	1	1.1	318	138	331	151	70
			320	140	333	153	66
			321	141	334	154	66
			315	135	328	148	64
			321	141	334	154	74
		1.2	314	134	327	147	72
			320	140	333	153	84
			317	137	330	150	86
		1.3	317	137	330	150	72
	3	3.1	318	138	331	151	72
			312	132	325	145	68
			315	135	328	148	64
			312	132	325	145	78
2.4	1	1.1	301	121	314	134	80
			305	125	318	138	80
			309	129	322	142	72
			337	157	350	170	80
			308	128	321	141	72
		1.2	307	127	320	140	78
			315	135	328	148	80
			313	133	326	146	70
			340	160	353	173	78
		1.3	340	160	353	173	56
		1.4	323	143	336	156	74
			317	137	330	150	68
			318	138	331	151	58
			329	149	342	162	52
			331	151	344	164	60

Table A4: F2 stikes and dips

Site	Traverse	Segment	Strike (°)	Strike - 180 (°)	Corrected (°)	Corrected - 180 (°)	Dip (°)
1.3	2	2.1	228	48	241	61	78
			232	52	245	65	80
			228	48	241	61	82
			234	54	247	67	84
			225	45	238	58	70
			226	46	239	59	-------
			226	46	239	59	72
			232	52	245	65	70
			277	97	290	110	-------
		2.3	238	58	251	71	78
			225	45	238	58	-------
			223	43	236	56	82
			241	61	254	74	86
			232	52	245	65	86
			226	46	239	59	-------
			233	53	246	66	-------
		2.4	220	40	233	53	88
			218	38	231	51	86
			231	51	244	64	88
			236	56	249	69	88
	4	4.1	221	41	234	54	86
			227	47	240	60	88
			238	58	251	71	82
			232	52	245	65	84
			233	53	246	66	80
			230	50	243	63	80
			232	52	245	65	89
		4.2	226	46	239	59	88
			217	37	230	50	88
			241	61	254	74	76
			244	64	257	77	76
			220	40	233	53	62
			236	56	249	69	82
		4.3	223	43	236	56	82
			238	58	251	71	82
			238	58	251	71	74
			231	51	244	64	78
			232	52	245	65	82
		4.4	221	41	234	54	84
			218	38	231	51	62
			215	35	228	48	88
			212	32	225	45	88
			234	54	247	67	78
1.4	2	2.1	238	58	251	71	72
			235	55	248	68	72
		2.2	233	53	246	66	62
		2.5	229	49	242	62	60
		2.6	234	54	247	67	77
			231	51	244	64	82
			229	49	242	62	80
		2.7	228	48	241	61	88
			248	68	261	81	68
		2.11	242	62	255	75	82
2.4	2	2.1	237	57	250	70	70
			237	57	250	70	[illegible]
			237	57	250	70	[illegible]
			237	57	250	70	[illegible]
			241	61	254	74	80
		2.2	231	51	244	64	88
		2.4	235	55	248	68	86
			231	51	244	64	88
		2.5	250	70	263	83	78
			244	64	257	77	80

Table A5: Google Earth Dataset 1

Site	Traverse	Spacing number	Northing (m)	Easting (m)	Spacing (m)	Spacing (cm)	Site	Traverse	Spacing number	Northing (m)	Easting (m)	Spacing (m)	Spacing (cm)
1.3	1	1	4278477.883	748379.3492	2.34950595	235	1.3	5	57	4278695.835	748098.2552	2.294186775	229
		2	4278477.012	748377.5372	2.010468851	201			58	4278695.476	748097.2379	1.07878649	108
		3	4278476.639	748376.8079	0.819150468	82			59	4278694.857	748095.4703	1.872850971	187
		4	4278476.206	748375.8626	1.039750494	104			60	4278694.266	748093.763	1.806697066	181
		5	4278474.784	748372.9259	3.262865442	326			61	4278693.858	748092.7385	1.102753032	110
		6	4278473.957	748371.3217	1.80482316	180			62	4278691.205	748092.786	1.390960935	139
		7	4278473.727	748370.8321	0.540932676	54			63	4278690.996	748092.1563	0.663478025	66
		8	4278473.197	748369.698	1.251831782	125			64	4278690.629	748091.1218	1.097669919	110
		9	4278472.83	748368.9163	0.863564641	86			65	4278689.432	748088.0213	3.323538664	332
		10	4278472.407	748368.1014	0.918145419	92			66	4278688.335	748085.1704	3.054675074	305
		11	4278472.033	748367.3024	0.882200091	88			67	4278685.489	748077.5714	8.114463445	811
		12	4278471.569	748366.3058	1.099321409	110			68	4278685.097	748076.59	1.056792298	106
		13	4278470.978	748365.0429	1.394344796	139			69	4278684.089	748073.9281	2.84636182	285
		14	4278470.539	748364.1937	0.955961108	96			70	4278683.326	748072.0169	2.057876196	206
		15	4278469.754	748362.6056	1.771520988	177			71	4278682.967	748070.9909	1.08699448	109
		16	4278461.648	748361.9686	4.153403748	415			72	4278682.438	748069.7784	1.322874616	132
		17	4278461.448	748361.5304	0.481683755	48			73	4278677.926	748059.4334	4.02762221	403
		18	4278459.615	748357.6041	4.33309597	433			74	4278677.469	748058.2186	1.297728567	130
		19	4278458.113	748354.5653	3.389735895	339			75	4278674.234	748050.2482	8.601931011	860
		20	4278455.66	748349.4816	5.644573916	564			76	4278673.872	748049.2397	1.071639634	107
		21	4278453.699	748345.385	4.541767559	454			77	4278672.743	748046.4595	3.000475309	300
		22	4278453.315	748344.6299	0.847131637	85			78	4278671.072	748042.3627	4.424723209	442
		23	4278452.516	748342.929	1.879218404	188			79	4278669.734	748039.0748	3.549578132	355
		24	4278441	748328.766	9.12153204	912			80	4277141.375	750079.454	1.539498909	154
		25	4278440.478	748327.8235	1.077399763	108	2.4	1	81	4277140.819	750077.9371	1.615587079	162
		26	4278439.74	748326.4692	1.542256004	154			82	4277140.348	750076.4088	1.599231656	160
	3	27	4277104.381	749999.4928	1.128224929	113			83	4277139.725	750074.8243	1.702577238	170
		28	4278574.035	748185.4168	1.673086921	167			84	4277139.071	750072.7089	2.214189052	221
		29	4278573.537	748184.6479	0.916293508	92			85	4277138.075	750069.7237	3.146972361	315
		30	4278572.716	748183.4444	1.456636099	146			86	4277136.943	750063.3864	6.045301913	605
		31	4278572.305	748182.7686	0.790942383	79			87	4277136.456	750061.9109	1.553791894	155
		32	4278571.606	748181.7967	1.197179993	120			88	4277135.463	750059.2569	2.833683998	283
		33	4278570.115	748179.6815	2.588004586	259			89	4277131.892	750049.1428	10.72599925	1073
		34	4278568.471	748177.1527	3.016260711	302			90	4277131.649	750048.514	0.674120494	67
		35	4278430.774	748320.4637	9.34453266	934			91	4277131.428	750047.8321	0.716818394	72
		36	4278425.599	748319.3956	2.440060124	244			92	4277131.132	750047.0655	0.821761255	82
		37	4278424.074	748316.0612	3.666585382	367			93	4277130.968	750046.6435	0.45274717	45
		38	4278418.583	748313.8089	1.923217731	192			94	4277131.204	750043.9423	2.154270492	215
		39	4278416.659	748309.6762	4.558616598	456			95	4277129.962	750040.9474	3.24221992	324
		40	4278416.033	748308.519	1.315670111	132			96	4277129.008	750038.7194	2.423654266	242
		41	4278415.591	748307.5914	1.027723172	103			97	4277128.667	750037.9541	0.837833569	84
		42	4278414.866	748306.0973	1.660509074	166			98	4277127.548	750035.1733	2.997500565	300
		43	4278414.572	748305.5137	0.653471469	65			99	4277126.692	750033.2037	2.147570758	215
		44	4278413.584	748303.2434	2.475965688	248			100	4277126.128	750031.8701	1.447958895	145
		45	4278701.782	748133.4568	1.852573065	185			101	4277116.506	750030.5062	2.326274733	233
	5	46	4278701.194	748132.002	1.569135762	157			102	4277114.388	750025.5074	5.428989357	543
		47	4278700.122	748129.3422	2.86770292	287			103	4277113.339	750022.9772	2.739035057	274
		48	4278699.187	748126.9221	2.594438092	259			104	4277112.542	750021.215	1.934052181	193
		49	4278698.682	748125.6739	1.346487371	135			105	4277112.165	750020.5468	0.767437253	77
		50	4278696.469	748120.0861	6.010064712	601			106	4277111.709	750019.2273	1.395933926	140
		51	4278694.879	748115.9519	4.429414142	443			107	4277111.133	750017.772	1.565143472	157
		52	4278694.366	748114.6867	1.365247245	137			108	4277110.123	750015.0662	2.888157482	289
		53	4278692.562	748110.1582	4.874600317	487			109	4277109.383	750013.0494	2.148274247	215
		54	4278698.039	748104.6626	1.397318399	140			110	4277107.445	750007.7137	5.676754221	568
		55	4278697.112	748102.0156	2.804627961	280			111	4277105.641	750002.8446	5.192547622	519
		56	4278696.569	748100.4288	1.677135427	168			112	4277104.792	750000.5435	2.452725465	245

Table A6: Google Earth Dataset 2

Site	Traverse	Spacing number	Northing (m)	Easting (m)	Spacing (m)	Spacing (cm)	Site	Traverse	Spacing number	Northing (m)	Easting (m)	Spacing (m)	Spacing (cm)
1.3	2	1	4278626.921	748205.4409	1.881471788	188	1.4	2	67	4275341.203	747963.2435	6.000180414	600
		2	4278626.037	748205.9739	1.032252392	103			68	4275353.231	747954.177	14.36082705	1436
		3	4278623.997	748207.1791	2.369410694	237			69	4275362.559	747948.5339	10.9021173	1090
		4	4278623.16	748207.6845	0.977751584	98			70	4275377.246	747939.4199	17.28505033	1729
		5	4278622.655	748207.9965	0.593606772	59			71	4275390.514	747950.7796	6.807538439	681
		6	4278617.095	748211.3245	6.479906173	648			72	4275395.708	747947.8981	5.939754056	594
		7	4278616.104	748211.9306	1.161653222	116			73	4275396.521	747947.5066	0.902353174	90
		8	4278614.983	748212.5843	1.297676651	130			74	4275397.793	747946.7783	1.465743801	147
		9	4278614.579	748212.8322	0.473994103	47			75	4275399.574	747945.7901	2.036786744	204
		10	4278613.045	748213.7601	1.792806295	179			76	4275401.704	747944.6341	2.423476016	242
		11	4278612.561	748214.0192	0.548988898	55			77	4275402.002	747944.3982	0.380069481	38
		12	4278611.521	748214.6268	1.204482362	120			78	4275408.169	747940.9632	7.059115667	706
		13	4278610.94	748214.9848	0.682440473	68			79	4275410.866	747939.3973	3.118629797	312
		14	4278610.361	748215.3514	0.685300344	69			80	4275412.967	747938.2596	2.389259778	239
		15	4278606.442	748217.7307	4.584716947	458			81	4275400.55	747902.4592	4.983801685	498
		16	4278594.619	748206.2881	2.8752976	288			82	4275405.036	747900.1315	5.053947298	505
		17	4278590.344	748208.9225	5.021522514	502			83	4275408.836	747898.0605	4.327706205	433
		18	4278587.873	748210.481	2.921431712	292			84	4275411.605	747896.5708	3.144291191	314
		19	4278586.728	748211.179	1.340980611	134			85	[illegible]	[illegible]	4.254861748	425
		20	4278585.879	748211.7457	1.020759468	102			86	[illegible]	[illegible]	12.12630081	1213
		21	4278584.051	748212.9182	2.171713666	217			87	4275430.758	747877.9626	9.223482437	922
		22	4278570.528	748221.4183	15.97246688	1597			88	4275431.866	747877.5184	1.193724273	119
		23	4278557.221	748201.698	0.803288641	80			89	4275435.679	747876.1795	4.041240181	404
		24	4278555.656	748202.7141	1.865927171	187			90	4275438.553	747880.3541	1.479956001	148
		25	4278552.198	748204.9309	4.107549908	411			91	4275439.154	747880.1698	0.628623488	63
		26	4278550.806	748205.8457	1.665689959	167			92	4275441.732	747879.5928	2.641782163	264
		27	4278550.405	748206.0935	0.471387144	47			93	4275444.087	747879.0403	2.418942176	242
		28	4278549.177	748206.8638	1.449602046	145			94	4275445.17	747878.8497	1.099644197	110
		29	4278547.294	748208.0729	2.237769383	224			95	4275446.448	747878.4875	1.328334611	133
		30	4278546.346	748208.6689	1.119785694	112			96	4275448.144	747878.1035	1.738928406	174
		31	4278545.708	748209.1071	0.773991757	77			97	4275449.586	747878.0675	1.442449306	144
		32	4278543.981	748210.1806	2.033453036	203			98	4275450.61	747877.9747	1.028196402	103
		33	4278543.195	748210.7105	0.947939876	95			99	4275451.364	747877.9339	0.755103066	76
		34	4278540.88	748212.177	2.740410052	274			100	4275454.689	747877.5605	3.345900859	335
		35	4278538.973	748213.352	2.239580209	224			101	4275456.808	747877.2855	2.136769992	214
		36	4278525.201	748192.2079	0.841671699	84			102	4275458.254	747877.1797	1.449865386	145
		37	4278524.185	748192.8495	1.201626631	120			103	4275459.33	747877.0591	1.082737439	108
		38	4278523.54	748193.2618	0.765517008	77			104	4275461.412	747876.8027	2.097728523	210
		39	4278522.161	748194.1327	1.630983694	163			105	4275462.86	747876.6968	1.451867354	145
		40	4278517.646	748196.853	5.27117227	527			106	4275470.796	747892.782	0.69411803	69
		41	4278515.048	748198.5026	3.077463916	308			107	4275472.512	747892.6067	1.724930749	172
	4	42	4278713.762	748155.9723	3.987717322	399			108	4275473.319	747892.5729	0.807707521	81
		43	4278714.691	748155.5424	1.023647893	102			109	4275474.505	747892.4926	1.188715311	119
		44	4278715.603	748155.0783	1.023295075	102			110	4275476.671	747892.2771	2.176693881	218
		45	4278716.558	748154.639	1.051194316	105			111	4275479.133	747892.1746	2.464132758	246
		46	4278719.414	748153.3562	3.130864392	313			112	4275489.736	747891.3226	10.63717599	1064
		47	4278721.486	748152.3679	2.295630826	230	2.4	2	113	4277136.108	750070.4914	2.933053905	293
		48	4278730.73	748148.1062	10.1790777	1018			114	4277135.61	750070.9255	0.660641211	66
		49	4278731.181	748147.9004	0.495736462	50			115	4277134.982	750071.4682	0.830004392	83
		50	4278731.753	748147.6299	0.632735529	63			116	4277133.559	750072.6722	1.864013143	186
		51	4278733.193	748146.9663	1.585548789	159			117	4277132.693	750073.4577	1.169173319	117
		52	4278721.539	748100.5332	4.442428756	444			118	4277130.692	750075.2203	2.666600788	267
		53	4278726.419	748098.1939	5.411721028	541			119	4277130.033	750075.7379	0.837968233	84
		54	4278740.882	748091.1205	16.10004213	1610			120	4277129.515	750076.2946	0.760420206	76
		55	4278742.96	748090.1844	2.279115444	228			121	4277127.681	750077.8253	2.388848779	239
		56	4278776.178	748122.3855	14.53083478	1453			122	4277127.068	750078.4112	0.847966868	85
		57	4278779.548	748120.6683	3.782284474	378			123	4277126.662	750078.7813	0.549372379	55
		58	4278784.522	748118.1779	5.562622417	556			124	4277126.329	750079.0445	0.424456405	42
		59	4278794.911	748112.7825	5.37196454	537			125	4277125.582	750079.7305	1.014201656	101
		60	4278803.17	748109.0047	9.082007148	908			126	4277125.048	750080.1482	0.677959652	68
		61	4278808.554	748106.5365	5.922792182	592			127	4277108.237	750081.6857	4.344443197	434
		62	4278817.919	748102.2624	10.294272	1029			128	4277096.037	750077.2118	9.613069751	961
1.4	2	63	4275326.388	747973.1288	18.87248161	1887			129	4277095.604	750077.4956	0.517717529	52
		64	4275328.314	747972.1186	2.174851728	217			130	4277095.208	750088.1089	5.247007121	525
		65	4275333.429	747969.4226	5.782010117	578			131	4277083.467	750089.2698	11.29307246	1129
		66	4275335.994	747966.2215	3.678817975	368							

Appendix B – Google Earth Dataset Collection

Traverse generation

Traverses in Google Earth are direct replications of their field counterpart and were generated with heading and coordinate info from the field (**Figure 16**). Once corrected for declination these coordinates were plotted with the *Add Placemark* tool (**Figure 16**). Once selected, a placemark is generated and its properties displayed where coordinates may be directly input. *Add Path* may then be selected to connect the endpoints of a given segment.

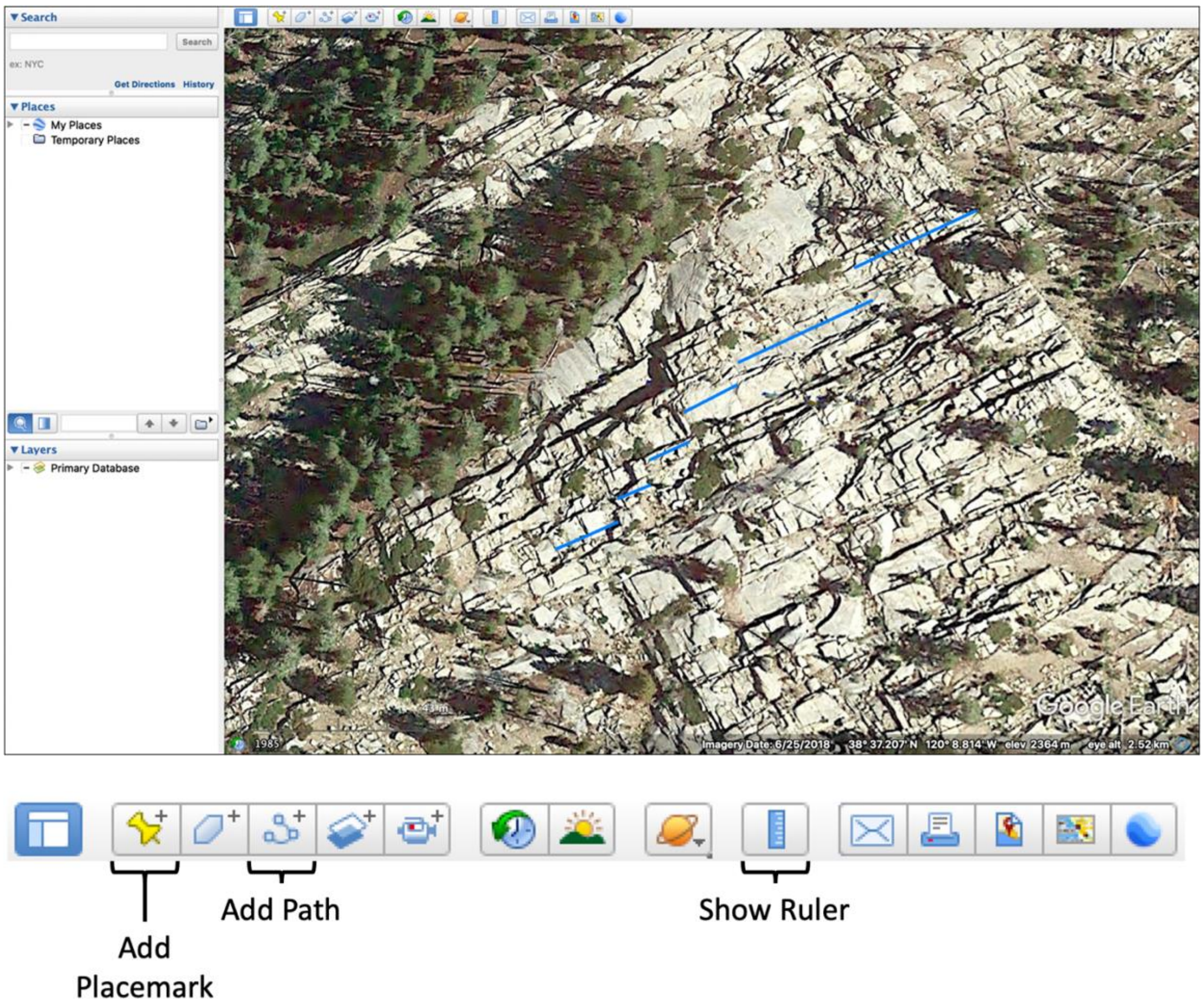

Figure 16. Google Earth window with traverse 1 at site 1.3 drawn. Closeup of toolbar indicates the tools used for data collection. From Google Earth.

These were then checked with the *Show Ruler* tool for length and heading.

Data collection

To collect the positions of intersection between joints and the traverse we again use the *Add Path* tool. A placemark may seem more intuitive, however, as shown in **Figure 17** the placemark itself makes accurate positioning difficult, no matter which style is used.

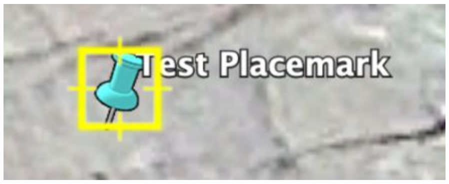

Figure 17. Issues related to using the placemark tool. Taken from Google Earth.

Google Earth paths are instead comprised of a sequence of points and each point is associated with a given set of coordinates. Therefore, each position of intersection can be recorded with one point of one path (it was later realized that an entire segment could then have been sampled by one singular path with multiple points) (**Figure 18**).

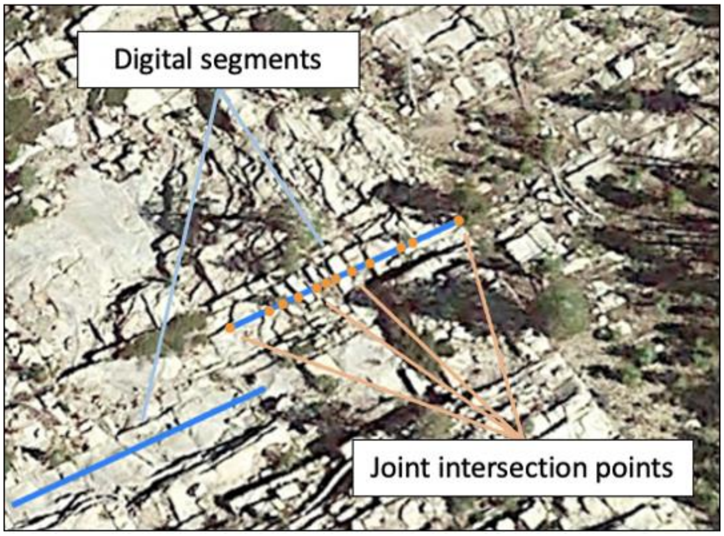

Figure 18. Zoomed in photo of **Figure 16** showing points assigned to intersections. The size of each point is exaggerated. Taken from Google Earth.

If the beginning or end of the traverse is not intersected by a joint in the imagery its position needs to be recorded. The reasoning is illustrated in **Figure 19**. This figure considers two hypothetical traverse segments (blue) that sample a joint set (black). The position of intersection of each joint is designated by a green dot. If we were to calculate the spacing between each of these, we would also calculate the length of the diagonal between the segments (yellow, dashed) instead of spacings along their length. This sampled "spacing" is longer than the true spacing and can be avoided my recording the position of the end and beginning of the segments (blue dots).

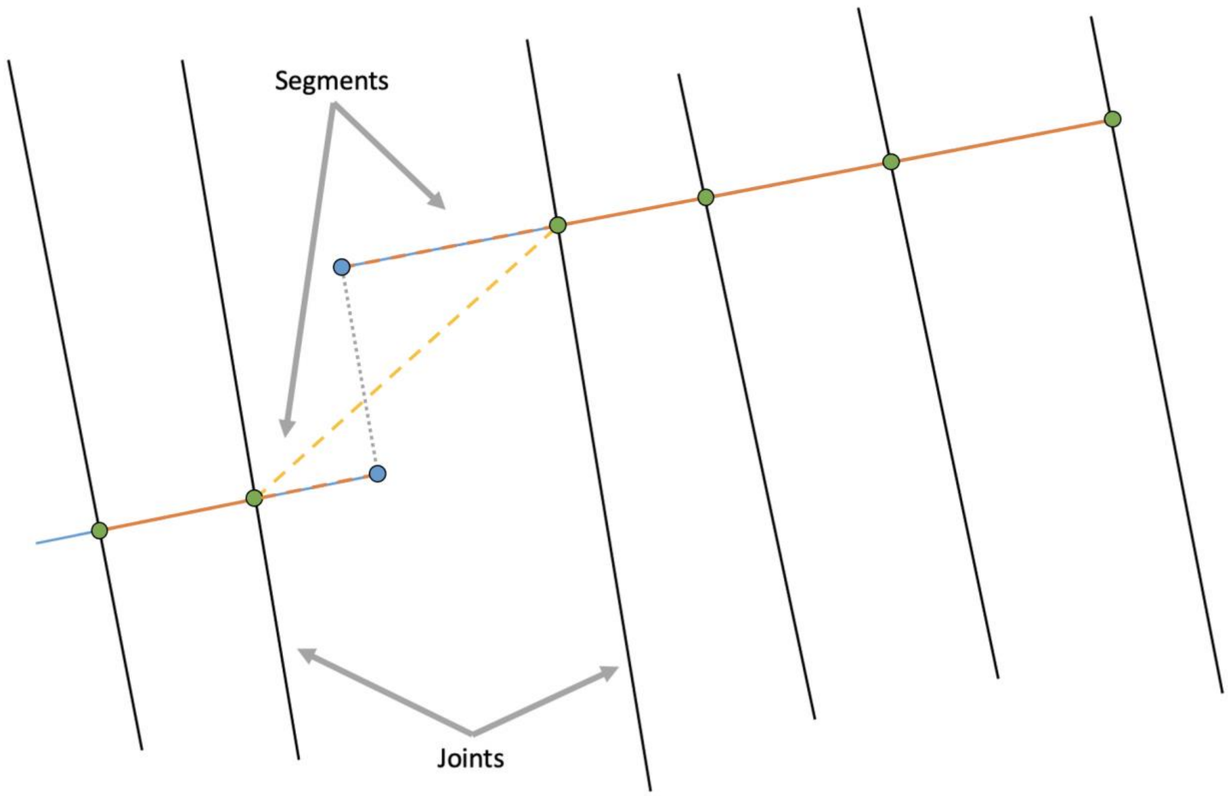

Figure 19. Simple schematic showing the necessity of recording traverse endpoints.

Data conversion

Data related to each intersection was then exported as in .kml (Keyhole Markup Language) format—exporting in this fashion just saves the coordinate data in latitude and longitude. We cannot easily determine spacing in these units and so we convert them into

Universal Transverse Mercator (UTM) coordinates, northing and easting, with units of meters. Spreadsheets can be set up to do this, but we used online batch converters via https://consult.hermes.com.np/batch-convert-lat-long-to-utm.

Spacing calculation

Spacing between each datapoint was determined through with algebraic distance equation between two points, $d = \sqrt{(n_f - n_i)^2 + (e_f - e_i)^2}$, where (n_f, e_f) are the coordinates of the jth joint and (n_i, e_i) those of the ith, in northing and easting respectively. For spacings that cover the end of a segment and the start of the next two of these calculations need to be made and then summed accordingly.

Appendix C – Statistical Methodology

Chi-squared (χ^2) goodness-of-fit

The Chi-squared test determines if a population has a certain theoretical distribution. This is based on how well the expected frequencies of the hypothesized distribution—in this case lognormal, normal, gamma, or exponential—fit the true, observed frequencies of the data. Goodness-of-fit is determined by the quantity,

$$\chi^2 = \sum_{i=1}^{k} \frac{(o_i - e_i)^2}{e_i},$$

where o_i and e_i are the observed and expected frequencies of the ith to the kth bin, respectively. Through this value we are then equipped to accept or reject the null hypothesis (H_0: the spacing distribution is the one being tested against). A poor fit is indicated by a large χ^2—rejection of the null—a good fit is indicated by a small value—therefore leading to acceptance (Walpole et al., 2012).

Frequencies (and bins) were derived through a small series of steps. First, we generate stem-and-leaf plots from the data. These plots constitute a tabular and graphic way of presenting large masses of statistical data and can be quite useful for simple characterizations (Walpole et al., 2012). As an example, consider the sample dataset in **Figure 20** below. Here we have 40 arbitrary values arranged by sampling order. To gather these into a more approachable format we may split each quantity into a stem and leaf. For example, 4.1 below can be separated into a stem of 4 and a leaf of 1, 3.5 into a stem of 3 and leaf of 5, and so on. In this way stems effectively function as bins and we may associate a frequency to each. Below, the "1" stem has 2 leaves; therefore, it has a frequency of 2. Now, spreadsheet commands can acquire this information much more conveniently whereas the above method is essentially determining frequency by hand. In this case, the latter was chosen to provide a more comprehensive first approach to the statistical analysis of geologic data. If the reader is especially familiar with statistical methods, they may easily determine frequencies via more computational methods.

2.2	4.1	3.5	4.5	3.2	3.7	3.0	2.6
3.4	1.6	3.1	3.3	3.8	3.1	4.7	3.7
2.5	4.3	3.4	3.6	2.9	3.3	3.9	3.1
3.3	3.1	3.7	4.4	3.2	4.1	1.9	3.4
4.7	3.8	3.2	2.6	3.9	3.0	4.2	3.5

Stem	Leaf	Frequency
1	69	2
2	25669	5
3	0011112223334445567778899	25
4	11234577	8

Figure 20. Example stem-and-leaf plot generated from arbitrary data. Adapted from Walpole et al., (2012).

Stems are chosen are somewhat arbitrarily, but it is generally accepted that a greater number will provides a more representative picture of the distribution and, usually, between 5-20 are set (Walpole et al., 2012). Our choice for stems is not as straightforward given the magnitude and range of our values, but since we solely seek their frequencies, we are satisfied with a much greater number. Datasets 1 and 2 were initially separated into 103 and 143 stems, respectively (the first stem is “0” to account for all spacings less than 10 cm). Leaves can be conveniently generated with Excel functions and we used the *REPT* as well as *COUNTIF*. The first will repeat a specified string of text a specified number of times and the second will tell you the number of times a specified string is found within a specified array. For a single cell this must be done for each leaf you wish to display. For example,

= REPT("0",COUNTIF(if in data, there exists 1*10+0)) &

REPT("1",COUNTIF(if in data, there exists 1*10+1)) &

REPT("2",COUNTIF(if in data, there exists 1*10+2)) &

…

&

…

REPT("9",COUNTIF(if in data, there exists 1*10+9)),

will display all the leaves of the first stem, 1, for all values in your dataset (spacings) from 10-19 cm. **Tables C1** and **C2** show the stem-and-leaf plots for field datasets 1 and 2.

Table C1: Field dataset 1 stem-and-leaf plot

Stem	Leaf	Stem	Leaf
0	1 1 1 1 1 2 2 2 2 2 2 2 3 3 3 3 3 3 3 3 3 3 3 3 3 3 3 4 4 4 4 4 4 4 4 4 4 4 4 5 5 5 5 5 5 5 5 5 5 5 6 6 6 6 6 6 6 6 6 7 7 7 7 7 7 7 7 8 8 8 8 8 8 8 8 8 8 8 9 9	52	
1	0 1 1 1 1 1 2 2 2 2 2 3 3 4 4 4 4 4 4 5 5 5 5 6 6 7 8 8 8 8 8 8 9 9 9 9 9 9	53	
2	0 0 1 1 1 1 1 1 1 2 4 4 4 5 6 6 7 7 7 8 9	54	
3	0 0 1 2 3 3 3 5 6 7 8 8 9	55	
4	0 0 1 1 5 7 7 9	56	
5	0 1 2 3 3 3 4 4	57	4 5 9
6	0 1 1 2 2 3 3 3 4 8 9	58	
7	2 5 5 6 7 7 8 8 8 9 9	59	
8	2 3 4 4 6 7 7 8 9 9 9	60	
9	0 0 0 4 7 9	61	
10	0 4 9	62	
11	0 2 3 7 9	63	
12	3 3 7	64	
13	0 3 3 5 7 7 7	65	
14	0 0 5 6	66	
15	2 4	67	
16	1 6 7	68	1 7
17	1 2 2 7 9	69	
18	2 4 8	70	
19	6	71	
20	5 6 7 8	72	
21	1 6 6 9	73	
22	0 5	74	3
23	0 7 8	75	
24	3 5 6	76	
25		77	7
26	1 1	78	
27	2 7 8 9	79	
28	5	80	
29	3	81	
30	0 7	82	
31	8 9	83	
32	1	84	
33	0 0 7	85	
34		86	
35	9	87	
36	1	88	
37	7	89	
38		90	
39		91	
40		92	
41		93	3
42		94	
43		95	
44		96	
45	3 3 6	97	
46		98	
47		99	
48		100	
49	4	101	
50		102	0
51			

Table C2: Field dataset 2 stem-and-leaf plot

Stem	Leaf	Stem	Leaf
0	1 1 1 1 1 2 2 2 2 2 3 3 3 3 3 3 4 4 4 4 4 5 5 5 6 6 6 6 7 7 7 7 8 8 8 8 8 9 9 9 9	72	9
1	0 0 0 1 1 1 1 2 2 2 3 3 3 4 4 4 4 4 4 4 5 5 5 6 7 8 8 8 8 8 9 9	73	
2	0 0 1 2 3 4 4 4 5 5 6 7 8 8 9 9 9	74	
3	0 1 2 2 2 3 3 3 3 4 4 5 6 6 6 7 8 9	75	
4	0 0 1 3 3 4 6 6 7 7 7 9	76	
5	2 2 4 4 6 6 8 8 8	77	7
6	0 0 1 2 3 3 7 9	78	1
7	1 1 1 2 2 3 5 5 5 6 8 8 9	79	
8	4 6 6 7 9	80	3
9	0 0 0 2 6 8	81	
10	3 5 5 5 7 8 9	82	
11	0 2 8 8 9	83	
12	1 3 3 6 8	84	
13	1 3 5 6	85	
14	0 2 5 8	86	8
15	2 5 7	87	
16	1	88	
17	2 6	89	6
18	2	90	
19	3 4 6 9	91	
20	5 5	92	
21	1 2 3 4 6 6 9	93	
22	0 1 5	94	
23	5 7 7	95	1
24		96	
25	3 4	97	
26	1 1 4	98	
27	7 7	99	7
28	3 6	100	
29	4	101	
30	0 0	102	0
31		103	
32	1 8	104	
33	0 7	105	
34	0 6	106	
35	0 9	107	
36	1 4	108	
37	3 5	109	8
38		110	
39	3 5	111	8
40		112	
41		113	
42		114	
43	5 9	115	
44		116	
45	6	117	
46	2 3 6 8	118	
47		119	5
48		120	
49	0 8	121	
50	0 8	122	
51	2 8 8	123	
52	2	124	5
53		125	
54		126	
55	1	127	
56	5	128	
57	2 4	129	
58	1	130	
59		131	
60		132	
61		133	
62		134	
63		135	
64	0	136	
65	0	137	
66		138	
67		139	
68	1	140	
69		141	
70		142	6
71			

From there we calculate the frequency of each stem to build the frequency distribution. Here, we now consolidate frequencies into bins and separate each dataset into around 20, as generally accepted (Walpole et al., 2012). The expected frequencies of each bin are then calculated with the distribution function. For example, for the lognormal test of dataset 1 we would execute this command,

= LOGNORM.DIST(49, mean, standard deviation, TRUE)* sample size.

This yields the projected lognormal distribution of our spacing data from 0-49 cm based off of the required parameters—mean and standard deviation. Here, TRUE is a conditional statement that indicates we desire the cumulative distribution. For subsequent calculations TRUE would recalculate the frequencies from each previous bin so we must modify our command to,

= LOGNORM.DIST(99, mean, standard deviation, TRUE) –

LOGNORM.DIST(50, mean, standard deviation ,TRUE))* sample size.

The subtraction negates this resampling and only leaves behind the distribution between 50-99 cm, or the next bin. See **Tables C3** and **C2**.

Table C3: Field dataset 1 frequency distribution

Class interval	Observed (o)	Expected (e)
0-49	161	171.0
50-99	47	45.3
100-149	22	21.4
150-199	14	12.5
200-249	16	8.1
250-299	8	5.6
300-349	8	4.1
350-399	3	3.1
400-449	0	2.4
450-499	4	1.9
500-549	0	1.6
550-599	3	1.3
600-649	0	1.1
650-699	2	0.9
700-749	1	0.8
750-799	1	0.7
800-849	0	0.6
850-899	0	0.5
900-949	1	0.5
950-999	0	0.4
1000-1049	1	0.4

Table C4: Field dataset 2 frequency distribution

Class interval	Observed (o)	Expected (e)
0-49	120	119.0
50-99	41	47.3
100-149	25	25.5
150-199	11	16.1
200-249	15	11.1
250-299	10	8.1
300-349	8	6.2
350-399	8	4.9
400-449	2	3.9
450-499	7	3.2
500-549	6	2.7
550-599	5	2.2
600-649	1	1.9
650-699	2	1.6
700-749	1	1.4
750-799	2	1.3
800-849	1	1.1
850-899	2	1.0
900-949	0	0.9
950-999	2	0.8
1000-1049	1	0.7
1050-1099	1	0.6
1100-1149	1	0.6
1150-1199	1	0.5
1200-1249	1	0.5
1250-1299	0	0.4
1300-1349	0	0.4
1350-1399	0	0.4
1400-1449	1	0.3

In some cases, bins must be further consolidated so that they have a frequency of at least 5. With less, the criterion which ultimately leads to rejection or acceptance of the null may be inaccurate. The remaining number of bins will define our degrees of freedom, $\nu = k - 1$, where k is the number of bins (Walpole et al., 2012). With this we may finally determine the critical value of our test. We use the table from Walpole et al. (2012), attached, at a level of significance of 0.05.

If the calculated test value (χ^2) was greater than the critical, we are led to rejection, if less, we fail to reject. P-values were also calculated to corroborate our findings and can simply be defined as the probability of obtaining that Chi-squared value. In general, if greater than the level of significance we accept, if less we reject.

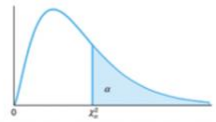

Table A.5 Critical Values of the Chi-Squared Distribution

	α									
v	0.995	0.99	0.98	0.975	0.95	0.90	0.80	0.75	0.70	0.50
1	0.0^4393	0.0^3157	0.0^3628	0.0^3982	0.00393	0.0158	0.0642	0.102	0.148	0.455
2	0.0100	0.0201	0.0404	0.0506	0.103	0.211	0.446	0.575	0.713	1.386
3	0.0717	0.115	0.185	0.216	0.352	0.584	1.005	1.213	1.424	2.366
4	0.207	0.297	0.429	0.484	0.711	1.064	1.649	1.923	2.195	3.357
5	0.412	0.554	0.752	0.831	1.145	1.610	2.343	2.675	3.000	4.351
6	0.676	0.872	1.134	1.237	1.635	2.204	3.070	3.455	3.828	5.348
7	0.989	1.239	1.564	1.690	2.167	2.833	3.822	4.255	4.671	6.346
8	1.344	1.647	2.032	2.180	2.733	3.490	4.594	5.071	5.527	7.344
9	1.735	2.088	2.532	2.700	3.325	4.168	5.380	5.899	6.393	8.343
10	2.156	2.558	3.059	3.247	3.940	4.865	6.179	6.737	7.267	9.342
11	2.603	3.053	3.609	3.816	4.575	5.578	6.989	7.584	8.148	10.341
12	3.074	3.571	4.178	4.404	5.226	6.304	7.807	8.438	9.034	11.340
13	3.565	4.107	4.765	5.009	5.892	7.041	8.634	9.299	9.926	12.340
14	4.075	4.660	5.368	5.629	6.571	7.790	9.467	10.165	10.821	13.339
15	4.601	5.229	5.985	6.262	7.261	8.547	10.307	11.037	11.721	14.339
16	5.142	5.812	6.614	6.908	7.962	9.312	11.152	11.912	12.624	15.338
17	5.697	6.408	7.255	7.564	8.672	10.085	12.002	12.792	13.531	16.338
18	6.265	7.015	7.906	8.231	9.390	10.865	12.857	13.675	14.440	17.338
19	6.844	7.633	8.567	8.907	10.117	11.651	13.716	14.562	15.352	18.338
20	7.434	8.260	9.237	9.591	10.851	12.443	14.578	15.452	16.266	19.337
21	8.034	8.897	9.915	10.283	11.591	13.240	15.445	16.344	17.182	20.337
22	8.643	9.542	10.600	10.982	12.338	14.041	16.314	17.240	18.101	21.337
23	9.260	10.196	11.293	11.689	13.091	14.848	17.187	18.137	19.021	22.337
24	9.886	10.856	11.992	12.401	13.848	15.659	18.062	19.037	19.943	23.337
25	10.520	11.524	12.697	13.120	14.611	16.473	18.940	19.939	20.867	24.337
26	11.160	12.198	13.409	13.844	15.379	17.292	19.820	20.843	21.792	25.336
27	11.808	12.878	14.125	14.573	16.151	18.114	20.703	21.749	22.719	26.336
28	12.461	13.565	14.847	15.308	16.928	18.939	21.588	22.657	23.647	27.336
29	13.121	14.256	15.574	16.047	17.708	19.768	22.475	23.567	24.577	28.336
30	13.787	14.953	16.306	16.791	18.493	20.599	23.364	24.478	25.508	29.336
40	20.707	22.164	23.838	24.433	26.509	29.051	32.345	33.66	34.872	39.335
50	27.991	29.707	31.664	32.357	34.764	37.689	41.449	42.942	44.313	49.335
60	35.534	37.485	39.699	40.482	43.188	46.459	50.641	52.294	53.809	59.335

Table A.5 (continued) Critical Values of the Chi-Squared Distribution

	α									
v	0.30	0.25	0.20	0.10	0.05	0.025	0.02	0.01	0.005	0.001
1	1.074	1.323	1.642	2.706	3.841	5.024	5.412	6.635	7.879	10.827
2	2.408	2.773	3.219	4.605	5.991	7.378	7.824	9.210	10.597	13.815
3	3.665	4.108	4.642	6.251	7.815	9.348	9.837	11.345	12.838	16.266
4	4.878	5.385	5.989	7.779	9.488	11.143	11.668	13.277	14.860	18.466
5	6.064	6.626	7.289	9.236	11.070	12.832	13.388	15.086	16.750	20.515
6	7.231	7.841	8.558	10.645	12.592	14.449	15.033	16.812	18.548	22.457
7	8.383	9.037	9.803	12.017	14.067	16.013	16.622	18.475	20.278	24.321
8	9.524	10.219	11.030	13.362	15.507	17.535	18.168	20.090	21.955	26.124
9	10.656	11.389	12.242	14.684	16.919	19.023	19.679	21.666	23.589	27.877
10	11.781	12.549	13.442	15.987	18.307	20.483	21.161	23.209	25.188	29.588
11	12.899	13.701	14.631	17.275	19.675	21.920	22.618	24.725	26.757	31.264
12	14.011	14.845	15.812	18.549	21.026	23.337	24.054	26.217	28.300	32.909
13	15.119	15.984	16.985	19.812	22.362	24.736	25.471	27.688	29.819	34.527
14	16.222	17.117	18.151	21.064	23.685	26.119	26.873	29.141	31.319	36.124
15	17.322	18.245	19.311	22.307	24.996	27.488	28.259	30.578	32.801	37.698
16	18.418	19.369	20.465	23.542	26.296	28.845	29.633	32.000	34.267	39.252
17	19.511	20.489	21.615	24.769	27.587	30.191	30.995	33.409	35.718	40.791
18	20.601	21.605	22.760	25.989	28.869	31.526	32.346	34.805	37.156	42.312
19	21.689	22.718	23.900	27.204	30.144	32.852	33.687	36.191	38.582	43.819
20	22.775	23.828	25.038	28.412	31.410	34.170	35.020	37.566	39.997	45.314
21	23.858	24.935	26.171	29.615	32.671	35.479	36.343	38.932	41.401	46.796
22	24.939	26.039	27.301	30.813	33.924	36.781	37.659	40.289	42.796	48.268
23	26.018	27.141	28.429	32.007	35.172	38.076	38.968	41.638	44.181	49.728
24	27.096	28.241	29.553	33.196	36.415	39.364	40.270	42.980	45.558	51.179
25	28.172	29.339	30.675	34.382	37.652	40.646	41.566	44.314	46.928	52.619
26	29.246	30.435	31.795	35.563	38.885	41.923	42.856	45.642	48.290	54.051
27	30.319	31.528	32.912	36.741	40.113	43.195	44.140	46.963	49.645	55.475
28	31.391	32.620	34.027	37.916	41.337	44.461	45.419	48.278	50.994	56.892
29	32.461	33.711	35.139	39.087	42.557	45.722	46.693	49.588	52.335	58.301
30	33.530	34.800	36.250	40.256	43.773	46.979	47.962	50.892	53.672	59.702
40	44.165	45.616	47.269	51.805	55.758	59.342	60.436	63.691	66.766	73.403
50	54.723	56.334	58.164	63.167	67.505	71.420	72.613	76.154	79.490	86.660
60	65.226	66.981	68.972	74.397	79.082	83.298	84.58	88.379	91.952	99.608

Kolmogorov-Smirnov

The K-S test fundamentally works the same way as the Chi-squared when the goal is to accept or reject a null hypothesis—that both sample distributions come from the same population. In this case we compare the fit between two cumulative distributions as explained in the methodology. The test value is their maximum difference between the bins of their cumulative frequencies. The critical value is can be calculated via,

= SQRT (- LN(alpha / 2)*0.5)* SQRT((sample size of F1 + sample size of F2)/(sample size of F1 * sample size of F2).

Table C5: F1-F2 cumulative frequency distributions

Class interval	F1	F2	CF1	CF2	Difference
0-49	161	120	0.5514	0.4364	0.1150
50-99	47	41	0.7123	0.5855	0.1269
100-149	22	25	0.7877	0.6764	0.1113
150-199	14	11	0.8356	0.7164	0.1193
200-249	16	15	0.8904	0.7709	0.1195
250-299	8	10	0.9178	0.8073	0.1105
300-349	8	8	0.9452	0.8364	0.1088
350-399	3	8	0.9555	0.8655	0.0900
400-449	0	2	0.9555	0.8727	0.0828
450-499	4	7	0.9692	0.8982	0.0710
500-549	0	6	0.9692	0.9200	0.0492
550-599	3	5	0.9795	0.9382	0.0413
600-649	0	1	0.9795	0.9418	0.0376
650-699	2	2	0.9863	0.9491	0.0372
700-749	1	1	0.9897	0.9527	0.0370
750-799	1	2	0.9932	0.9600	0.0332
800-849	0	1	0.9932	0.9636	0.0295
850-899	0	2	0.9932	0.9709	0.0222
900-949	1	0	0.9966	0.9709	0.0257
950-999	0	2	0.9966	0.9782	0.0184
1000-1049	1	1	1.0000	0.9818	0.0182
1050-1099	0	1	1.0000	0.9855	0.0145
1100-1149	0	1	1.0000	0.9891	0.0109
1150-1199	0	1	1.0000	0.9927	0.0073
1200-1249	0	1	1.0000	0.9964	0.0036
1250-1299	0	0	1.0000	0.9964	0.0036
1300-1349	0	0	1.0000	0.9964	0.0036
1350-1399	0	0	1.0000	0.9964	0.0036
1400-1449	0	1	1.0000	1.0000	0.0000
Total	**292**	**275**			

REFERENCES

Bai, T., & Pollard, D. D. (2000). Fracture spacing in layered rocks: a new explanation based on the stress transition. *Journal of Structural Geology, 22*, 43-57.

Bateman, P. C. (1968). Geologic Structure and History of the Sierra Nevada. *UMR Journal – VH McNutt Colloquium Series, 1*(8), 121-131.

Bertrand, L., Géraud, Y., Le Garzic, E., Place, J., Diraison, M., Walter, B., & Haffen, S. (2015). A multiscale analysis of a fracture pattern in granite: A case study of the Tamariu granite, Catalunya, Spain. *Journal of Structural Geology, 78*, 52-66.

Boadu, F. K., & Long, L. T. (1994). Statistical Distribution of Natural Fractures and the Possible Physical Generating Mechanism. *Pure and Applied Geophysics, 142*(2), 273-293.

Bonnet, E., Bour, O., Odling, N. E., Davy, P., Main, I., Cowie, P. & Berkowitz B. (2001). Scaling of Fracture Systems in Geological Media. *Reviews of Geophysics, 39*(3), 347-383.

Busby, C. J, DeOreo, S. B., Skilling, I., Gans, P. B., & Hagan, J. C. (2008). Carson Pass—Kirkwood paleocanyon system: Paleogeography of the ancestral Cascades arc and implications for landscape evolution of the Sierra Nevada (California). *GSA Bulletin, 120*(3/4), 274-299.

Cecil, M. R, Rotberg, G. L., Ducea, M. N., Saleeby, J. B., & Gehrels, G. E. (2012). Magmatic growth and batholitic root development in the Northern Sierra Nevada, California. *Geosphere, 8*(2), 592-606.

Clark, M. B., Brantley, S. L., & Fisher, D. M. (1995). Power-law vein-thickness distributions and positive feedback in vein growth. *Geology, 23*(11), 975-978.

Ehlen, J. (1999). Fracture characteristics in weathered granites. *Geomorphology, 31*, 29-45.

Ehlen, J. (2000). Fractal analysis of joint patterns in granite. *International Journal of rock Mechanics and Mining Sciences, 37,* 909-922.

Ericson, K, Migon, P., & Olvmo, M. (2004). Fractures and drainage in the granite mountainous area A study from Sierra Nevada, USA. *Geomorphology, 64*, 97-116.

Fatt, N. T. (1994). Joint spacings in granitic rocks of eastern Kuala Lumpur area, Peninsular Malaysia. *Geol. Soc. Malaysia, Bulletin, 35*, 157-168.

Fisher, G. B., Amos, C. B., Bookhagen, B., Burbank, D. W., & Godard, V. (2012). Channel widths, landslides, faults, and beyond: The new world order of high-spatial resolution Google Earth imagery in the study of earth surface processes. *Google Earth and Virtual Visualizations in Geoscience Education and Research: Geological Society of America Special Paper 492*, 1-22.

Fossen, H. (2016). *Structural Geology.* Cambridge University Press.

Gillespie, P. A., Walsh, J. J., Watterson, J., Bonson, C. G., & Manzocchi, T. (2000). Scaling relationships of joint and vein arrays from the Burren, Co. Clare, Ireland. *Journal of Structural Geology, 23*, 183-201.

Le Garzic, E., de L'Hamaide, T., Diraison, M., Géraud, Y., Sausse, J., de Urreiztieta, M., Hauville, B., Champanhet, J.-M. (2011). Scaling and geometric properties of extensional fracture systems in the Proterozoic basement of Yemen. Tectonic interpretation and fluid flow implications. *Journal of Structural Geology, 33*, 519-536.

Martel, S. J., Pollard, D. D., & Segall, P. (1988). Development of simple strike-slip fault zones, Mount Abbot quadrangle, Sierra Nevada, California. *Geological Society of America Bulletin, 100*, 1451-1465.

McCaffrey, K, Johnson, J. D., & Feely, M. (1993). Use of Fractal Statistics in the Analysis of Mo-Cu Mineralization at Mace Head, County Galway. *Irish Journal of Earth Sciences, 12*, 139-148.

McKee, E. H., Chaffee, M. A., Federspiel, F. E, McHugh, E. L., Cather, E. E., Scott, D. F., & Rumsey, C. M. (1982). Mineral Resource Potential of the Mokelumne Wilderness and Contiguous Roadless Areas, Central Sierra Nevada, California. *Department of the Interior United States Geological Survey.*

Morse, S., **Wood, J.**, & Maher, H. (2020). *Observing Fracture Patterns at 3 Scales in the Sierra Nevada Batholith, Mokelumne Wilderness, California.* Poster presentation, Geological Society of America Annual Meeting, 26-30 Oct., Online.

National Research Council. (1996). *Rock Fractures and Fluid Flow: Contemporary Understanding and Applications.* The National Academies Press.

Olson, J. E. (2004). Predicting fracture swarms – the influence of subcritical crack growth and the crack-tip process zone on joint spacing in rock. *Geological Society, London: Special Publications, 231*, 73-88.

Palinkas, L. A., Horwitz, S. M., Green, C. A., Wisdom, J. P., Duan, N., & Hoagwood, K. (2013). Purposeful sampling for qualitative data collection and analysis in mixed method implementation research. *Administration and Policy in Mental Health and Mental Health Services Research, 42*(5), 533-544.

Palmström, A. (1995). *RMi – a rock mass characterization system for rock engineering purposes* (400). [PhD Thesis, Oslo University].

Pennacchioni, G., & Zucchi, E. (2013). High temperature fracturing and ductile deformation during cooling of a pluton: The Lake Edison granodiorite (Sierra Nevada batholith, California). *Journal of Structural Geology, 50*, 54-81.

Pollard, D. D., & Aydin, A. (1988). Progress in understanding jointing over the past century. *Geological Society of America Bulletin, 100*, 1181-1204.

Pollard, D. D., & Martel, S. J. (2020). *Structural Geology: A Quantitative Introduction.* Cambridge University Press.

Reches, Z. (1986). Network of shear faults in the field and in experiment. *Annals of the Israel Physical Society: Fragmentation, Form, and Flow in Fractured Media*, *8*, 42-51.

Rouleau, A., & Gale, J. E. (1985). Statistical characterization of the fracture system in the Stripa Granite, Sweden. *International Journal of rock Mechanics and Mining Sciences*, *22*, 353-367.

Ruf, J. C., Rust, K. A., & Engelder, T. (1997). Investigating the effect of mechanical discontinuities on joint spacing. *Tectonophysics, 295,* 245-257.

Ryan, J. (2000). Fracture spacing and orientation distributions for two-dimensional data sets. *Journal of Geophysical Research*, *105*(B8), 19,305-19,320.

Segall, P., & Pollard D. D. (1983). Joint formation in granitic rock of the Sierra Nevada. *Geological Society of America Bulletin, 94*, 563-575.

Sierra Nevada Mountain Range Geomorphology. (2012, August). Geocaching. Retrieved February 2, 2021, from https://www.geocaching.com/geocache/GC3RQEW_sierra-nevada-mountain-range-geomorphology?guid=a86a1cb7-fd0a-4d08-813a-9fc3928d4ebb

Sendek, C. (2016). *Zircon Geochemical and Isotopic Constraints on the Evolution of the Mount Givens Pluton, Central Sierra Nevada Batholith* (4777). [Master's thesis, San Jose State University]. SJSU ScholarWorks.

Sousa, L. M. O. (2010). Evaluation of joints in granitic outcrops for dimension stone exploitation. *Quarterly Journal of Engineering Geology and Hydrology, 43,* 85-94.

Velde, B., Dubois, J., Moore, D., & Touchard, G. (1991). Fractal patterns of fractures in granites. *Earth and Planetary Science Letters, 104,* 25-35.

Walpole, R. E., Myers, R. H., Myers, S. L., & Ye. Keying. (2012). *Probability & Statistics for Engineers & Scientists.* Prentice Hall.

Wong, L. N. Y., Lai, V. S. K., Tam, T. P. Y. (2018) Joint spacing distribution of granites in Hong Kong. *Engineering Geology, 245,* 120-129.